Pergamon

Journal of Structural Geology, Vol. 20, No. 11, pp. 1455 to 1475, 1998

PII: S0191-8141(98)00045-5

0191-8141/98 $ - see front matter

Overthrust shear deformation of a foreland basin; structural studies south-east of the Pelvoux massif, SE France

JUDITH BÜRGISSER and MARY FORD

Geologisches Institut, ETH-Zentrum, CH-8092 Zürich, Switzerland

(*Received* 11 *December* 1997; *accepted in revised form* 29 *April* 1998)

Abstract—The Late Tertiary Champsaur–Prapic fold zone lies to the southeast of the Pelvoux basement massif in the footwall of the Frontal Pennine Thrust of the western Alps. The 0.8–1.3 km thick Late Eocene–Oligocene foreland basin succession lies directly on crystalline basement and was deformed by WSW-directed shear below the overthrusting internal alpine units on the Frontal Pennine Thrust. This deformation decouples from the basement in a top to WSW–SW basal shear zone. Above, the turbidite sequence (Grès du Champsaur) is folded in chevron-like folds. A 12 km long continuous profile across the Champsaur fold zone documents variations in chevron fold shape, axial plane dips and zonal distribution of folding which indicate progressively higher shear strains towards the Frontal Pennine Thrust in the east. Chevron fold axes trend generally NNW–SSE except close to the Pelvoux massif where fold axes curve to N–S possibly due to lateral drag. In the western part of the investigated area SW-directed thrusting on the Champsaur Thrust almost doubles the Tertiary stratigraphy. The Champsaur Thrust and chevron folding in its footwall deform the overlying internal thrust sheets. The Champsaur–Prapic fold zone is a particular example of overthrust shear deformation in the footwall of internal alpine nappes in which deformation is concentrated in diffuse ramp zones. To the north, late alpine deformation changes to WNW-directed partly post-dating the WSW–SW-directed deformation further south. Therefore, in the core of the external western Alpine arc, two sub-perpendicular transport directions which barely overlap can be distinguished.

INTRODUCTION

In external thrust belts, stratified sequences can become folded by simple shear within a broad shear zone, usually below an overthrusting mass. The resulting asymmetrical fold trains show a transition from upright to overturned folds and may describe larger asymmetric nappes. Such structures have been analysed in several external orogenic belts: e.g. in the Variscan belt of southwest England (Sanderson, 1979), from back-arc basin deposits in the southern Andes (Bruhn, 1979; Tanner and Macdonald, 1982), in the Helvetic Alps (Ramsay *et al.*, 1983; Dietrich and Casey, 1989; Rowan and Kligfield, 1992; Casey and Dietrich, 1997) and previously in the present study area by Plotto (1977) and Tricart (1980, 1984, 1986). This phenomenon has become known as overthrust shear. All these areas show some or all of the following characteristics: (1) folds show consistent facing and asymmetry across a large area, (2) there is a clear correlation between fold tightness and axial plane attitude which (3) both record a systematic increase in strain in one direction, (4) folds are non-cylindrical and (5) fold axis orientation is variable with respect to the stretching lineation (Gibson and Gray, 1985).

The issue of how folds are initiated in simple shear is problematic. The first mathematical and geometrical models for fold development in simple shear argue that to initiate folding in a shear zone the shear plane has to be initially at a low angle to the layering (Ghosh, 1966; Sanderson, 1979, 1982). However other authors have argued that to initiate folding in such a shear zone additional small perturbations are necessary within an anisotropic multilayer sequence on which folds can nucleate and amplify (Casey and Huggenberger, 1985). Alternatively, a fold can initiate when the bulk strain deviates from ideal simple shear for example, if there is a component of shortening parallel to the shear direction (Ridley and Casey, 1989). The progressive development of folds in a simple shear zone with a constant strain profile is shown in Fig. 1(a). Symmetrical buckle folds initiate by layer-parallel shortening with axial planes at a high angle to the shear zone (Sanderson, 1979) and subsequently rotate, tighten and become more asymmetrical as the strain increases. This model has been applied to asymmetrical fold trains where the folds are all of the same order (Bosworth and Vollmer, 1981; Tanner and Macdonald, 1982), being slightly modified to estimate shear strain by Gibson and Gray (1985) and Rowan and Kligfield (1992). In the case of the Millook nappe in southwest England (Sanderson, 1979) and the Helvetic nappes of Switzerland, folds record a marked increase in shear strain downwards across a large-scale recumbent nappe fold (Fig. 1b). For the Helvetic nappes, Ramsay *et al.*, (1983) proposed that the nappes were first emplaced over their footwall ramps to give a hanging wall anticline before the onset of progressive simple shear. Dietrich and Casey (1989) and Casey and Dietrich (1997) instead propose that these nappes evolved by contemporaneous superposition of pure shear and heterogeneous overthrust shear.

In this article asymmetrical folding is described and analysed from the Champsaur–Prapic fold zone which

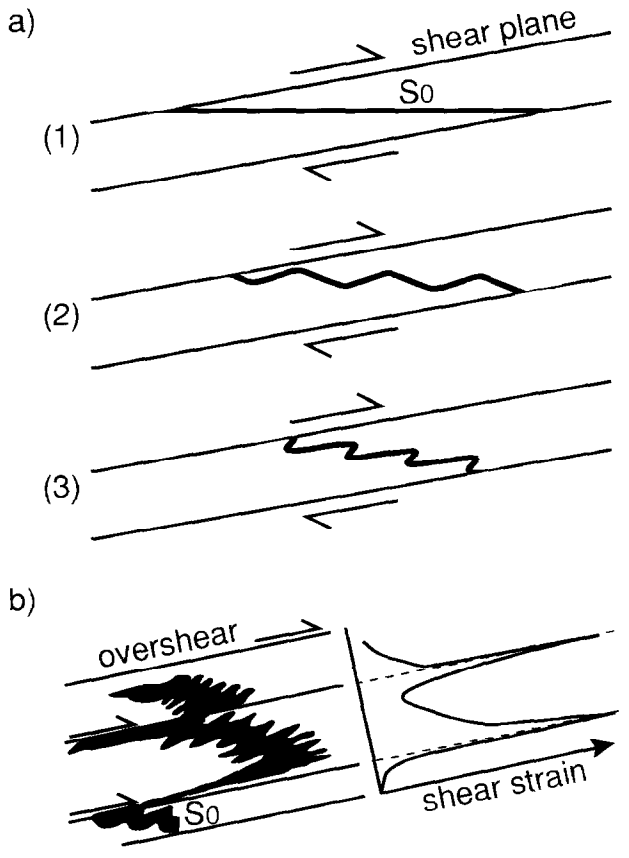

Fig. 1. Simplified cross sections of overthrust shear models: (a) Conceptual model of the progressive development of folds by simple shear (modified after Sanderson, 1979). (1) Undeformed geometry: a shear zone with a constant strain profile is at a low angle to layering; (2) initial generation of symmetric buckle folds; (3) development of asymmetry by passive rotation of axial planes. (b) Nappe geometry resulting from distributed simple shear originally oblique to the stratigraphic sequence (as in a) which concentrates at the lower nappe boundary (from card deck experiments). The graph to the right shows how the shear strain varies, the two peaks refer to the base of the nappes (modified after Casey and Dietrich, 1997).

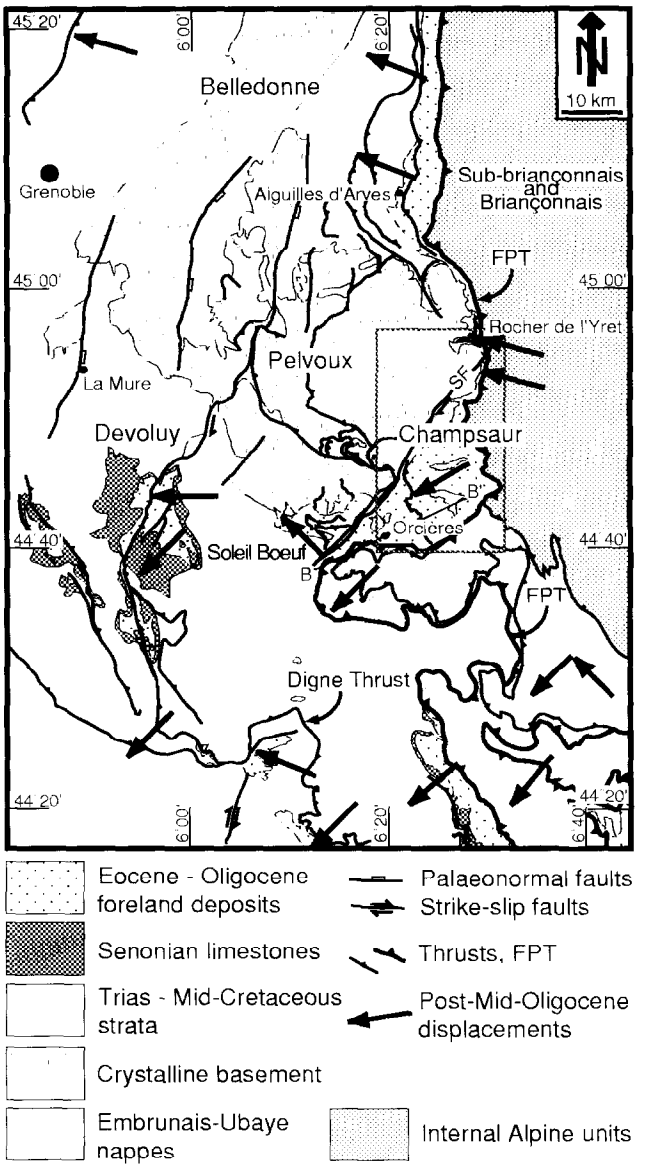

Fig. 2. Simplified geological map of SE France. Outline of Fig. 3 is shown. B–B' is the trace of the profile on Fig. 8. Tectonic transport directions are derived from the compilation of Platt *et al.* (1989) and the works of Arnaud *et al.* (1977), Butler (1992a), Meckel *et al.* (1996), and the authors' own field data. FPT = Frontal Pennine Thrust, SF = Selle-Fault.

lies in the footwall of the Frontal Pennine Thrust (FPT), the tectonic boundary between the external and internal units of the western Alps. The study area is divided in two by the Champsaur Thrust which separates the Champsaur fold zone and the Prapic fold zone. The Champsaur fold zone is underlain by the basal shear zone. The general geometries of asymmetrical chevron folds agree very well with the simple shear model of Sanderson (1979; Fig. 1a) and the characteristics of overthrust shear described above. However this area also has distinctive geometrical characteristics which suggest a more complex distribution of shear strain than shown in previous studies. Shear strain increases toward the hinterland indicating that it was generated by emplacement of the overriding internal thrust sheets with highest strains recorded at the rear. No major nappe folds have developed. Instead the deformation is concentrated in high strain zones which cut at a variable angle through sub-horizontal bedding, forming diffuse ramps linking floor and roof shear zones. The folds of Champsaur–Prapic have previously been mentioned in Gidon (1965) and described and analysed in the theses of Plotto (1977) and Tricart (1980). Their work is incorporated and discussed in this study.

Fig. 3. Simplified geological map of the Champsaur–Prapic fold zone adapted from BRGM maps 1:50,000 and the authors' own work. Arrows give fold axis orientation of chevron folds in the Grès du Champsaur. The fold axial trend is marked by thick grey lines. A–A' (note that the line is in two parts) and B–B' (see Fig. 2 for full section line) are the traces of the reconstructed profiles in Figs 5 and 8, respectively. CT = Champsaur Thrust; * = location of NNE–SSW trending open folds in basal shear zone; Y indicates the northern limit of observed F_{B2} folds.

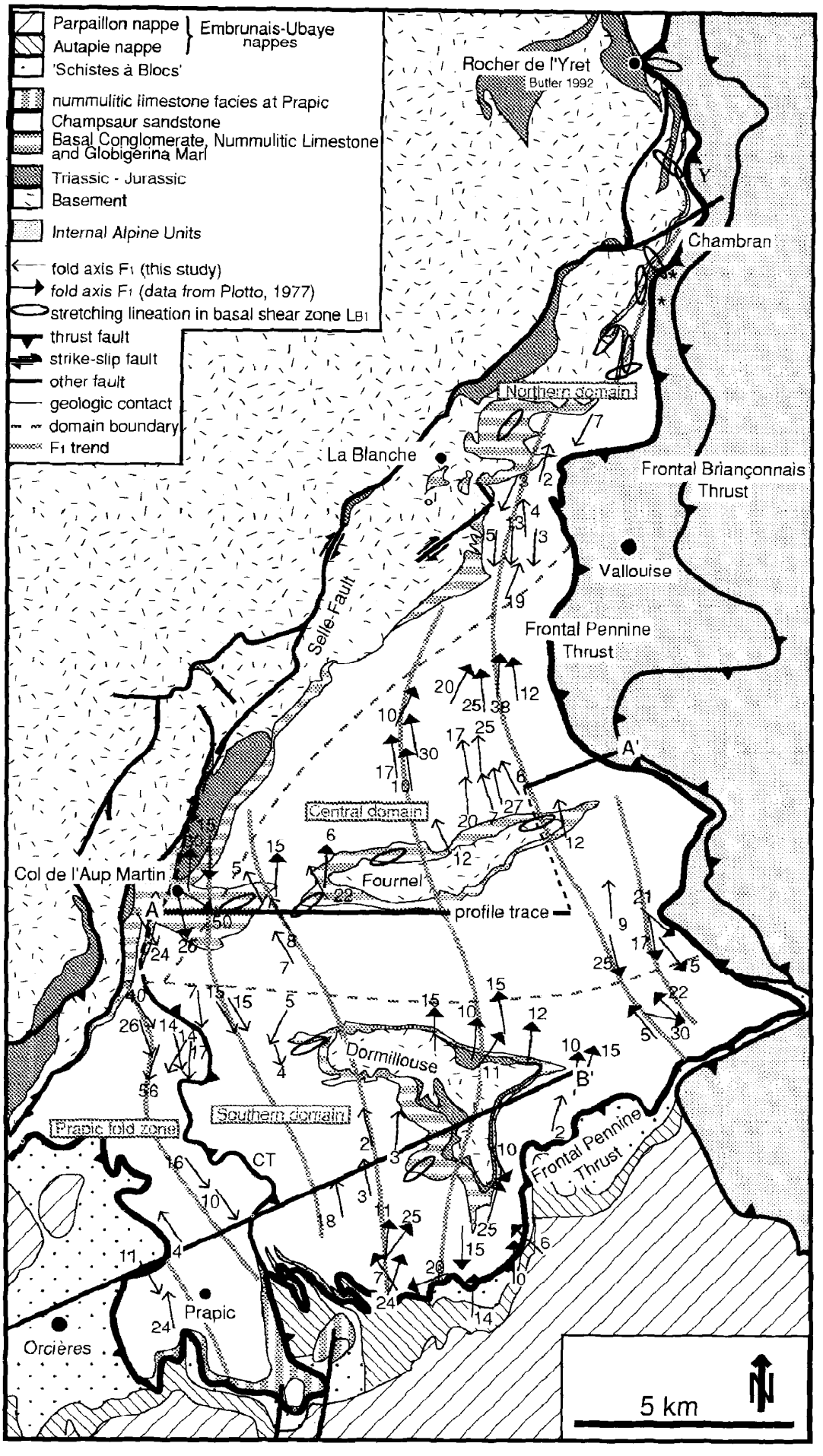
Parpaillon nappe
Autapie nappe
Embrunais-Ubaye nappes
'Schistes à Blocs'
nummulitic limestone facies at Prapic
Champsaur sandstone
Basal Conglomerate, Nummulitic Limestone and Globigerina Marl
Triassic - Jurassic
Basement
Internal Alpine Units
fold axis F1 (this study)
fold axis F1 (data from Plotto, 1977)
stretching lineation in basal shear zone LB1
thrust fault
strike-slip fault
other fault
geologic contact
domain boundary
F1 trend
Rocher de l'Yret
Butler 1992
Chambran
Northern domain
La Blanche
Frontal Briançonnais Thrust
Vallouise
Selle Fault
Frontal Pennine Thrust
Central domain
Col de l'Aup Martin
Fournel
profile trace
Dormillouse
Southern domain
Prapic fold zone
CT
Frontal Pennine Thrust
Prapic
Orcières
5 km

Fig. 3.

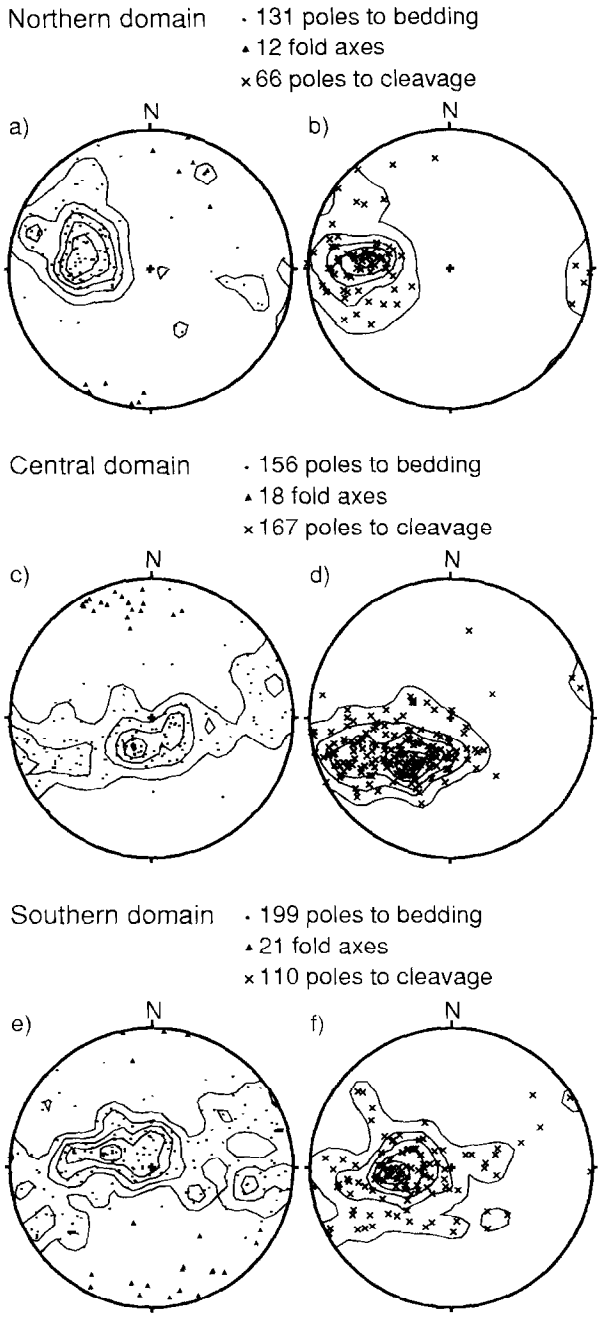

Fig. 4. Equal area lower hemisphere projections of structural elements (bedding, cleavage, fold axes) in the Grès du Champsaur turbidite sequence of (a) & (b) the northern domain, (c) & (d) the central domain and (e) & (f) the southern domain. Bedding poles and poles to cleavage are contoured at 1, 2, 3... times uniform. For further description see text.

GEOLOGICAL SETTING

The Champsaur–Prapic fold zone is situated at the southern rim of the Pelvoux basement massif (Fig. 2). It is covered by the 1:50,000 geologic maps of Orcières (Debelmas *et al.*, 1980), St-Christophe-en-Oisans (Barféty *et al.*, 1984), Briançon (Barféty *et al.*, 1995) and Guillestre (Debelmas *et al.*, 1966). A regional angular unconformity separates the strata of the southwestern Alpine foreland basin, from the Variscan crystalline basement and its relatively thin (< 1 km) remnants of Mesozoic cover. The Pelvoux basement and its Mesozoic cover were folded together by local Pyrenean Provençal events (Late Cretaceous to Eocene), uplifted and deeply eroded (Ford, 1996 and references therein), providing a rapidly varying substrate for the Tertiary sediments. The Late Eocene to Early Oligocene stratigraphy comprises local pockets of basal conglomerate (0–10 m), shallow water Nummulitic Limestone (5–50 m), hemipelagic Globigerina Marl (0–50 m) and turbiditic sandstones (700–1200 m), the Grès du Champsaur. The latter onlap their substrate from east to west. This sequence is typical of the underfilled stage of the foreland basin around the western Alpine arc (Sinclair, 1997).

The Champsaur–Prapic fold zone extends westward for some 14 km from the FPT (Fig. 3). The Champsaur Thrust separates the main Champsaur fold zone from the narrower Prapic fold zone to the west. No major folds occur in the Tertiary succession west of Orcières (south of the Selle-Fault; Fig. 2). For purposes of description, the Champsaur fold zone is divided into three domains: the central domain, including the Fournel basement inlier, the northern domain north of Vallouise and along the border to the Pelvoux massif and the southern domain, around the Dormillouse basement inlier and further south. Folds in the Grès du Champsaur record shear strain variations across the region while intense shear fabrics characterise the Globigerina Marl and the Nummulitic Limestone in the basal shear zone below.

The N–S-trending FPT separates the Tertiary sediments from the internal Sub-briançonnais units. Further east the Frontal Briançonnais Thrust carries the Briançonnais zone on top of the Sub-briançonnais zone (Fig. 3). Late normal displacements on both faults (Tricart *et al.*, 1996) probably thinned the Sub-briançonnais to a few metres in the Fournel valley (Fig. 3). To the south, the Tertiary sediments are tectonically overlain by the Embrunais Ubaye nappes, a more complex assemblage of Cretaceous Helminthoid flysch, Sub-briançonnais and Briançonnais units (Fig. 2). Structural and metamorphic evidence (Aprahamian, 1974; Bocquet, 1974; Waibel, 1990) indicate that internal thrust sheets overrode the whole Champsaur–Prapic fold zone. The sequence of emplacement of internal nappes over the foreland is complex and controversial and is beyond the scope of this article (Kerckhove, 1969; Tricart, 1980; Merle and Brun, 1984; Fry, 1989). The Embrunais–Ubaye nappes are separated from their foreland substrate by the 'Schistes à Blocs' (Fig. 3), described by Kerckhove (1969) as a marine sedimentary mélange implying that the submarine emplacement of the lowest of these nappes (Autapie) terminated foreland basin sedimentation. Kinematic data from the 'Schistes à Blocs' (see below) and other structural data (Lawson, 1987; Fry,

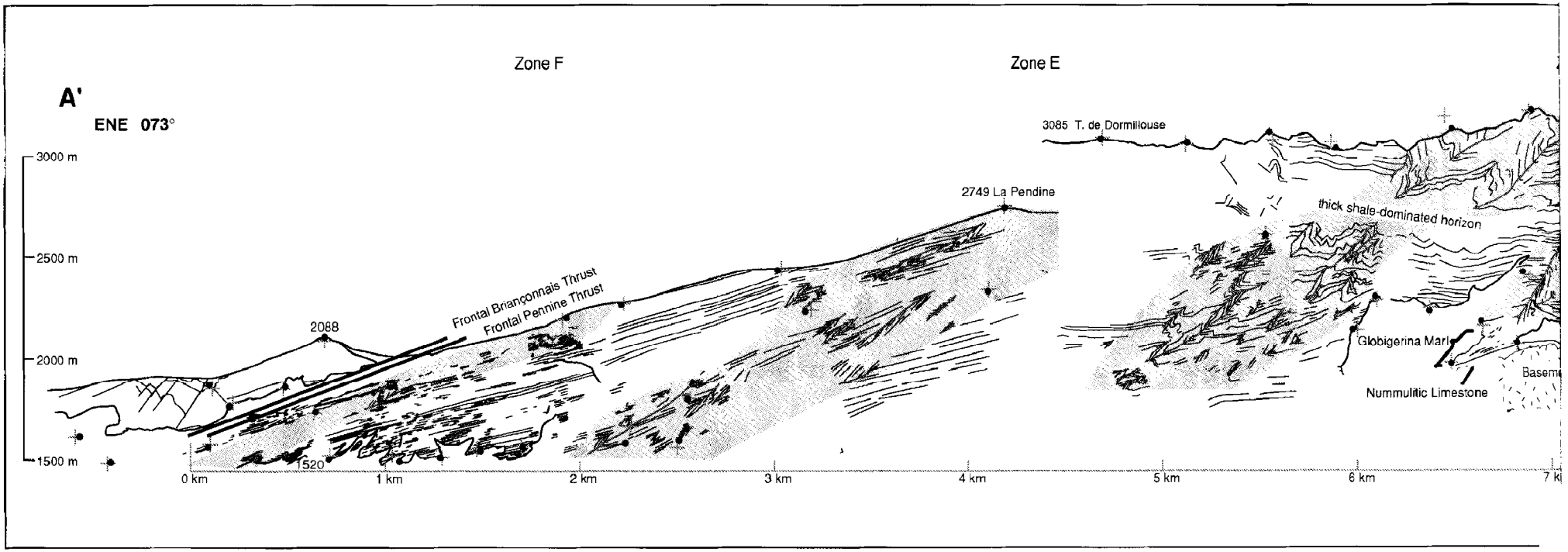

Fig. 5. Compiled and rectified ENE–WSW profile (location on Fig. 3) al
seven points was determined. These line drawings were then corrected for
photogrammetry, which calculates the ortho-projection on the best fit plan
order to correct for the inclination of the best fit plane, i.e. the inclination
point position (crosses) and the rectified fixed-point position (dots) give a
file plane perpendicular to the Π-fold axis. The eastern part of the final p
areas are zones of large-scale

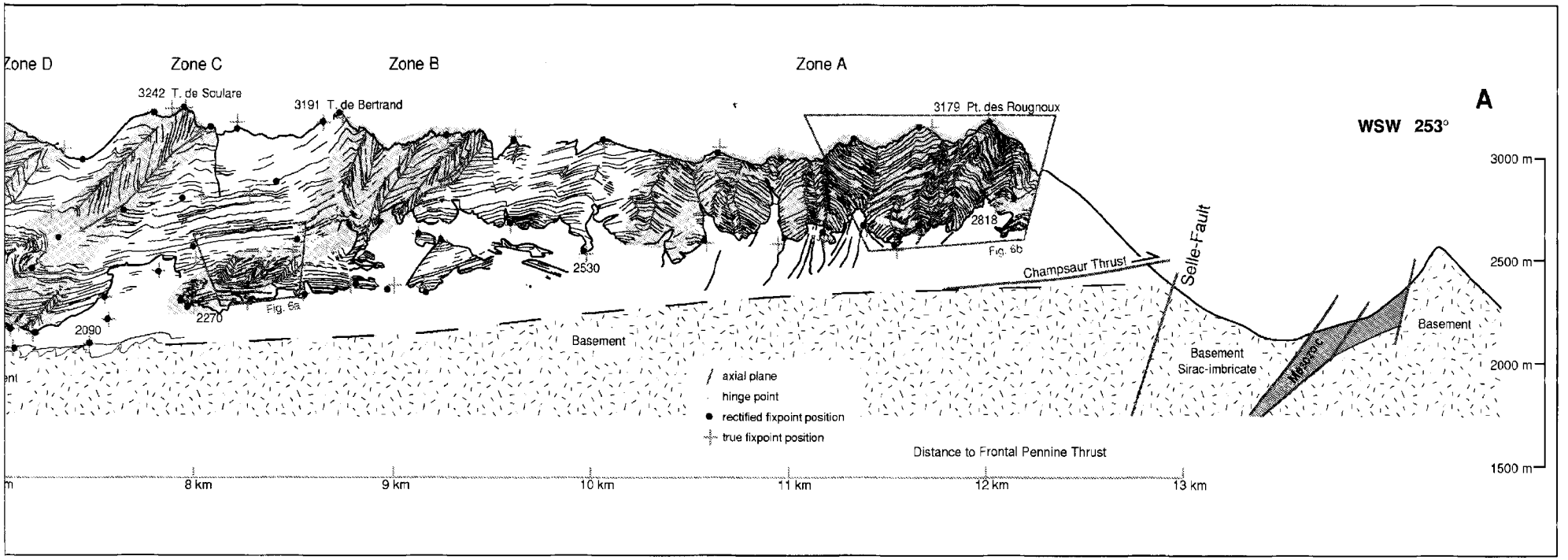

ong the Fournel valley. In each line drawing, made from field photographs, the exact location of about obliquity of camera view with respect to the cliff face by a digital façade rectification program, used in ne through the seven identified points. Each ortho-projection was then squeezed (in Adobe Illustrator) in of the cliff face. The corrected line drawings were then compiled to give the E–W profile. The true fixed- idea of the error involved. In the last step, the E–W profile was rotated 17° anticlockwise to give a pro- ofile is an inverted projection (parallel to the Π-fold axis 343-12), from the northern valley wall. Shaded folding (labelled A–F). Outlines of Fig. 6(a & b) are shown.

1989; Lickorish and Ford, 1998) show that the nappes were emplaced toward the SW–WSW (220°–240°).

Fission track studies (D. Seward, personal communication) indicate that uplift of the Pelvoux massif, like all other external basement massifs of the western Alps, has been ongoing since the Middle Miocene. This uplift has caused a steepening of all surfaces by up to 30° around the immediate southern and eastern borders of the massif. Differential uplift has been partially accommodated on the NNE–SSW trending Selle-Fault (Figs 2 & 3) (Plotto, 1977; Tricart, 1981).

On a more regional scale, the Champsaur–Prapic fold zone lies within the core of the external Alpine arc. Folding in Champsaur forms the northeasterly limit of the WSW-directed shortening of the Southern Subalpine chains (Malavieille *et al.*, 1984; Fry, 1989; Meckel *et al.*, 1996). WNW- to NW-directed shortening affects Tertiary strata in all regions to the north of the Pelvoux massif (e.g. Beach, 1980; Pijolat *et al.*, 1981; Gourlay, 1986; Coward *et al.*, 1991; Butler, 1992a; Spencer, 1992) and has been detected in this study at the northernmost corner of the Champsaur fold zone (Fig. 2). A zone of NW-directed deformation in Tertiary strata is also found in the Soleil Boeuf area (Lory, 1894; Gidon and Pairis, 1980–1981; Ford, 1996; Bürgisser and Ford, 1997) at the southwest corner of Pelvoux, to the north of the Selle-Fault (Fig. 2) and is the subject of current research.

THE CHAMPSAUR FOLD ZONE

The turbidite sequence consists of regular trains of gently plunging chevron folds. Individual folds die out laterally and cannot be traced for more than 4.5 km. Fold axes and axial trends, compiled from Plotto (1977) and this study, are shown on Fig. 3. A single axial planar cleavage is associated with the folds (Fig. 4). In the narrow northern domain, fold axes plunge toward N–NNE and S–SSW (Figs 3 & 4a). Poles to bedding and cleavage define similar cluster distributions, giving an average planar dip of 40–50° east, approximately parallel to the FPT (Fig. 4a & b). In the central domain fold axes plunge gently NNW and coincide well with the Π-pole (346-12) to the best fit great circle for bedding (Figs 3 & 4c). The elongate cluster of poles to axial planar cleavage (Fig. 4d & f) is generated by the east–west transition from moderately to steeply dipping axial planes. In the southern domain measured fold axes plunge dominantly to S–SSE but display a considerable scatter which is also reflected in the broad girdle distribution of poles to bedding (Figs 3 & 4e). Fold orientation can vary within a single fold pair suggesting that the folds may be weakly curvilinear in this region. In summary, fold axial trends curve from NNE in the northern domain to NNW in the central and southern domains. This curvature becomes more pronounced toward the east (Fig. 3).

The majority of folds show angles of axial transection Δ (Borradaile, 1978; Johnson, 1991) between +27° and −16°. The degree of axial transection may be related to fold trend: N–S to NW–SE folds tend to have smaller (or even negative) Δ-values than NE–SW-trending folds.

The northern domain

The northern domain is only 1–4 km wide and thus lateral variations in geometrical parameters of folds cannot be observed. In addition, this zone has been tilted 20–30° to the southeast by late uplift of the Pelvoux basement massif so that, for example, the dip of axial planes cannot be used to calculate shear strain. Interlimb angles however are not affected by later tilting and give a range similar to those of zones D–E in the central domain (see next paragraph).

The central domain: the Fournel profile

The southern side of the E–W Fournel valley (Fig. 3) provides an excellent 14 km long profile (from 1.5 to 0.8 km high) through the central domain from the FPT in the east to the Selle-Fault in the west. The valley cuts down into basement, thus exposing the basal shear zone in the lower Tertiary units (Fig. 3). This continuous profile, first documented by Plotto (1977), is re-drawn in more detail from rectified photographs for analysis of fold geometry (Fig. 5; see figure caption for details of correction procedure). Five zones of folding, labelled from A to F, with widths varying from 0.4 to 2 km are separated by zones 0.3–1.6 km wide of moderately east-dipping strata. The dip of the fold zones decreases from west to east (Fig. 5; Table 1).

Table 1. Geometric fold data from the Fournel profile (Fig. 5). ILA = fold interlimb angle. AP = fold axial plane. Shear strain $\gamma = \tan(90 - \alpha)$, where α is the dip of the axial plane

Fold zone	ILA range [°]	Average ILA [°]	Shortening $(l_0-l)/l_0$ [%]	Average AP-dip [°]	Shear strain γ	Average zone dip [°]
A	134–75	102	19	78	—	—
B	106–49	70	~36	50	0.9	~53–30
C	77–57	66	~46	40	1.1	48
D	90–26	54	~42	36	1.4	~32
E	55–22	34	65	32	1.7	28
F	101–26	63	—	41	—	20

(a)

(b)

Fig. 6. Field photographs (located on Fig. 5): (a) Isolated asymmetric chevron fold train bordered by shale-dominated shear horizons (fold duplex). View towards the south, width of view ~370 m. (b) Upright chevron folds from zone A. View towards the south. Width of view ~1000 m.

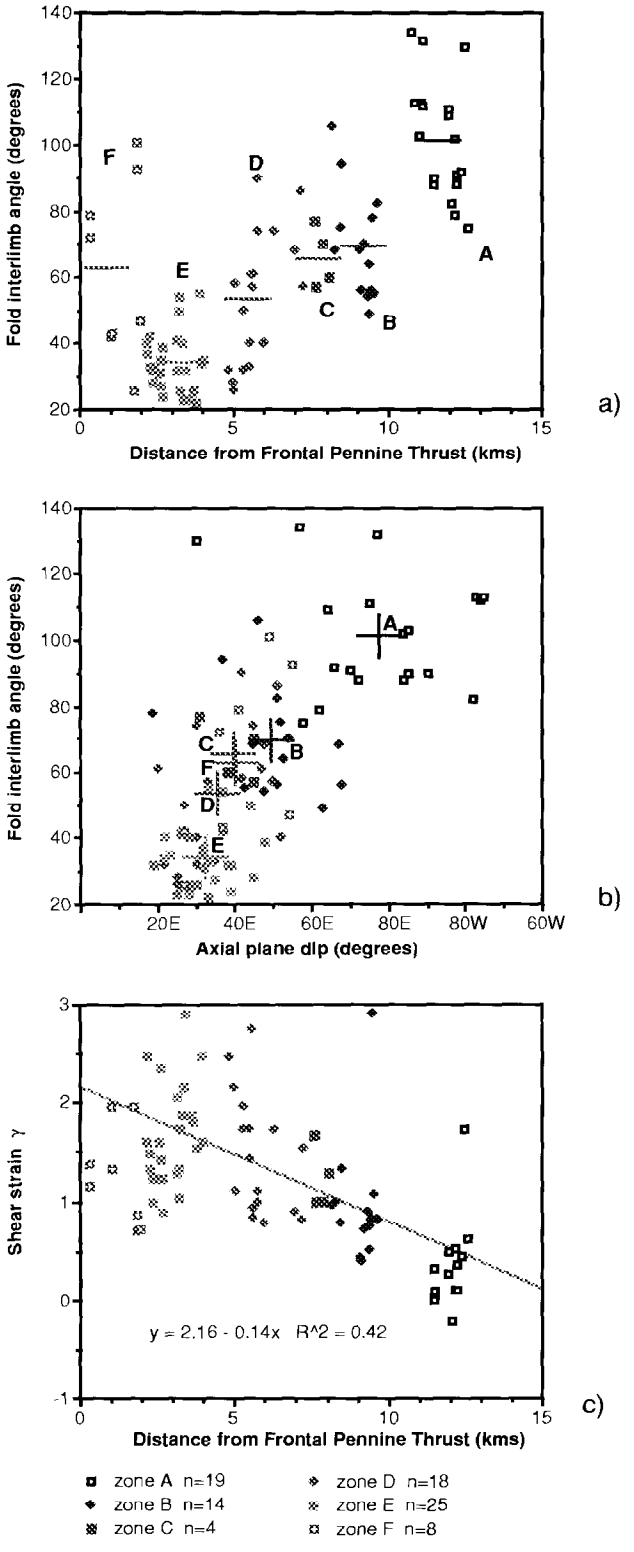

Fig. 7. Plots of geometric parameters of the Fournel chevron folds (Fig. 5). (a) Fold interlimb angle vs distance from a fixed point on the Frontal Pennine Thrust in the east. Horizontal bars represent the mean values of fold interlimb angles calculated for each inclined fold zone A–F. They decrease gradually towards the Frontal Pennine Thrust, with the exception of zone F in the immediate footwall of the thrust. (b) Fold interlimb angle vs axial surface dip of the same folds. Crosses represent the mean values for each zone. They show a linear relationship except for zones E and F which are bent down below the Frontal Pennine Thrust. (c) Shear strain ($\gamma = \tan(90 - \alpha)$, where α is the dip of the axial plane; Sanderson, 1979), vs distance from a fixed point on the Frontal Pennine Thrust. The curve was calculated without the data from zone F and extrapolated to the Frontal Pennine Thrust. For further explanation see text.

The size of folds is controlled largely by the percentage of sandstone and shale within the turbiditic succession and the thickness of sandstone- and shale-dominated packages. Wavelengths range between 50 and 450 m, amplitudes from 30 to 200 m. The typical chevron forms have long straight limbs, narrow hinge zones, rounded hinges in sandstone-dominated facies and angular hinges in mudstone-dominated facies (Fig. 6a). Limb-thrusts and hinge-collapse are relatively common in upright chevron folds (Fig. 6b). In sections with strongly marked layer thickness variations, the fold limbs become curved. The fold enveloping surface dips gently west. In the east it dips eastward below the Sub-briançonnais units.

Table 1 summarises the main geometrical features of the five fold zones and Fig. 7 (a & b) presents plots of fold interlimb angle vs distance from the FPT and interlimb angle vs axial plane dip. Two main trends characterise the deformation: mean interlimb angle and mean fold axial surface dip both decrease from west to east, together with an increase in relative shortening across the fold zones (calculated using bed length). The observed axial plane rotation and fold tightening are consistent with progressive non-coaxial deformation. Using the axial planes as passive markers that rotated from an original dip of 90° toward the shear direction with increasing shear (Sanderson, 1979), variation in shear strain within each fold zone (Table 1; Fig. 7c) was calculated. Although individual fold zones show a wide range of shear strains (Fig. 7c) the mean value clearly increases toward the east. However zone F does not fit with this trend. In this zone axial planes have become parallel to the FPT. As they can no longer rotate they cannot be used to calculate shear strain. One best fit line is constructed through these data (excluding zone F) and extrapolated to find the shear strain at the FPT. The line gives a shear strain of 2.2 at the FPT. This is a minimum estimate. Bulk fold shortening in this profile is ~22%. Plotto (1977) estimated 30% because he assumed that folding was homogeneously developed across the region.

In the westernmost zone A, fold axial planes dip steeply east or west. Folds are tighter in the west than in the east (Fig. 7a) indicating that they were either tightened against the Pelvoux massif or by a later activity on the Selle-Fault. Within the fold zones themselves shear strain tends to increase downward (Zones B and D), however deformation is strongly affected by mechanical stratigraphy and thus no consistent vertical variation in strain can be detected. For example, shear strain clearly increases at the thick shale-dominated horizon in zones B, C and D, as shown by the narrow-

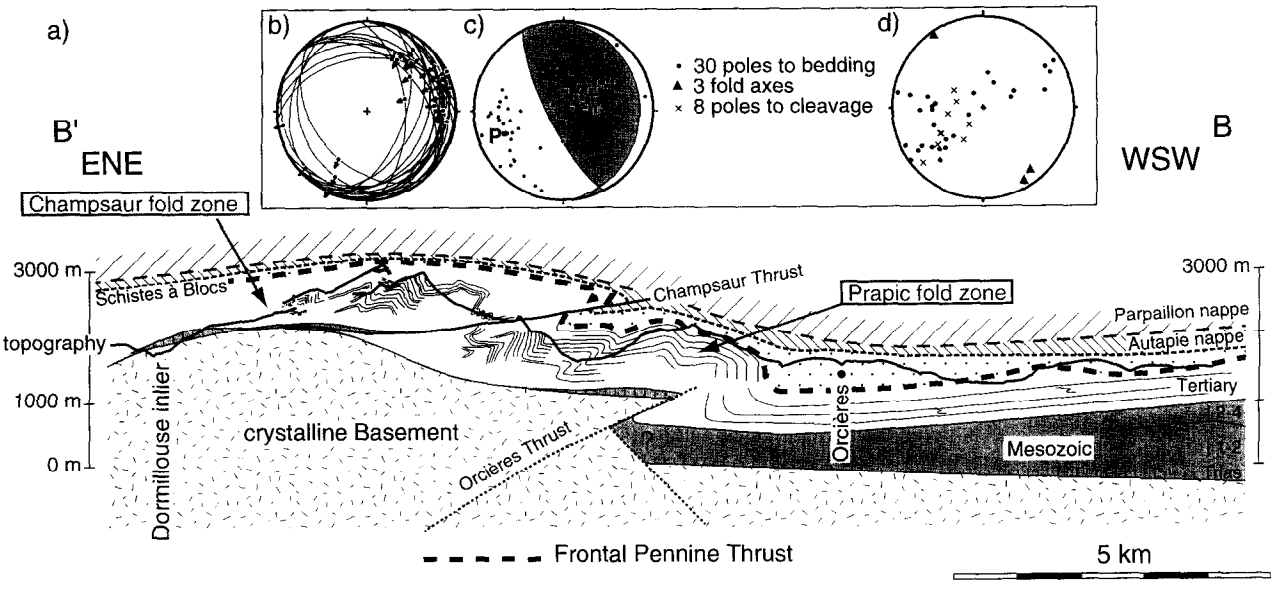

Fig. 8. (a) ENE–WSW profile (localised in Figs 2 & 3) across the Dormillouse basement inlier and the Champsaur Thrust. The strong deformation in the footwall of the Champsaur Thrust rapidly dies out towards the WSW. The change from basement-dominated substrate to thick Mesozoic substrate is related to a Mesozoic half graben structure. j 1–2 = marly limestones (Bajocian–Lower Bathonian), j 2–4 = Terres Noires (Upper Bathonian–Oxfordian). The stratigraphy of the Embrunais–Ubaye nappes (Parpaillon and Autapie) is Upper Cretaceous–Palaeocene. For further discussion see text. (b) Equal area lower hemisphere projection plots of fault kinematic data from the Schistes à Blocs around Orcières. (c) Fault plane solutions derived with the FaultKin programme of Allmendinger (1989–1994). Showing the P and T axes for individual slip surfaces (n = 29) and the mean P (055-59) and T (248-30) axes for the data set. (d) Structural elements (bedding, cleavage, fold axis) in the turbidite sequence Grès du Champsaur from the footwall of the Champsaur Thrust.

ing and flattening of the fold zones as they cross this level. There are also individual fold packages bounded by unfolded but sheared shale-rich horizons (Fig. 6a). The fold package in Fig. 6(a) displays all the features of a duplex, but without discrete thrust surfaces. Axial surfaces are sigmoidal and, towards the shale-rich beds above and below, fold amplitude and interlimb angle decrease.

The southern domain

In the southern domain, folds in the Grès du Champsaur, observed around the Dormillouse basement inlier, record a similar strain gradient to that in the central domain. Figure 8(a) depicts the western part in the hanging wall of the Champsaur Thrust with the transition from asymmetric to upright chevron folds. Interlimb angle and axial plane dip both decrease from west to east (Fig. 9a & b). The calculated shear strain thus increases toward the FPT giving a minimum value of $\gamma = 2.3$ at the fault itself (Fig. 9c).

THE PRAPIC FOLD ZONE

The Prapic fold zone lies in the footwall of the Champsaur Thrust (Figs 3 & 8). The Champsaur Thrust dips 10–30° east and can be traced northward where it links to the basal shear zone (Figs 3 & 5). Displacement on the Champsaur Thrust decreases northward.

In the Dormillouse area, the Champsaur Thrust almost doubles the Tertiary stratigraphy and the thrust is marked by a sudden change in chevron fold morphology (Fig. 8a). In the hanging wall, close to the thrust plane, chevron folds become overturned and minor asymmetric folding affects the limbs. In the footwall the turbidite sequence is folded in large tight recumbent asymmetrical SW-vergent folds. All folds have subhorizontal fold axes trending NW–SE (145°; Fig. 8d). Most of the deformation is accommodated in a narrow (~3 km) zone in the footwall of the thrust. Restoration of bed lengths give at least 1 km shortening in this zone. The orientation and vergence of these folds suggest that they were generated during southwesterly movement on the Champsaur Thrust.

To explain the presence of nummulitic limestone facies at the base of the 'Schistes à Blocs' south of Prapic (Fig. 3) Kerckhove *et al.*, (1978) propose an early large-scale recumbent nappe-like syncline, overturned towards the northwest (well illustrated on the 1:50,000 geologic map of Orcières; Debelmas *et al.*, 1980). They describe overturned bedding in the underlying turbidites to represent a major upper overturned fold limb. In the present study, no evidence for such an overturned fold was found (Fig. 8a). We therefore suggest that this nummulitic limestone sequence is either part of the 'Schistes à Blocs' or the overlying Sub-briançonnais sequence. A nummulitic limestone unit in a similar tectonic position has been described above the turbidites of the Aiguilles d'Arves north of

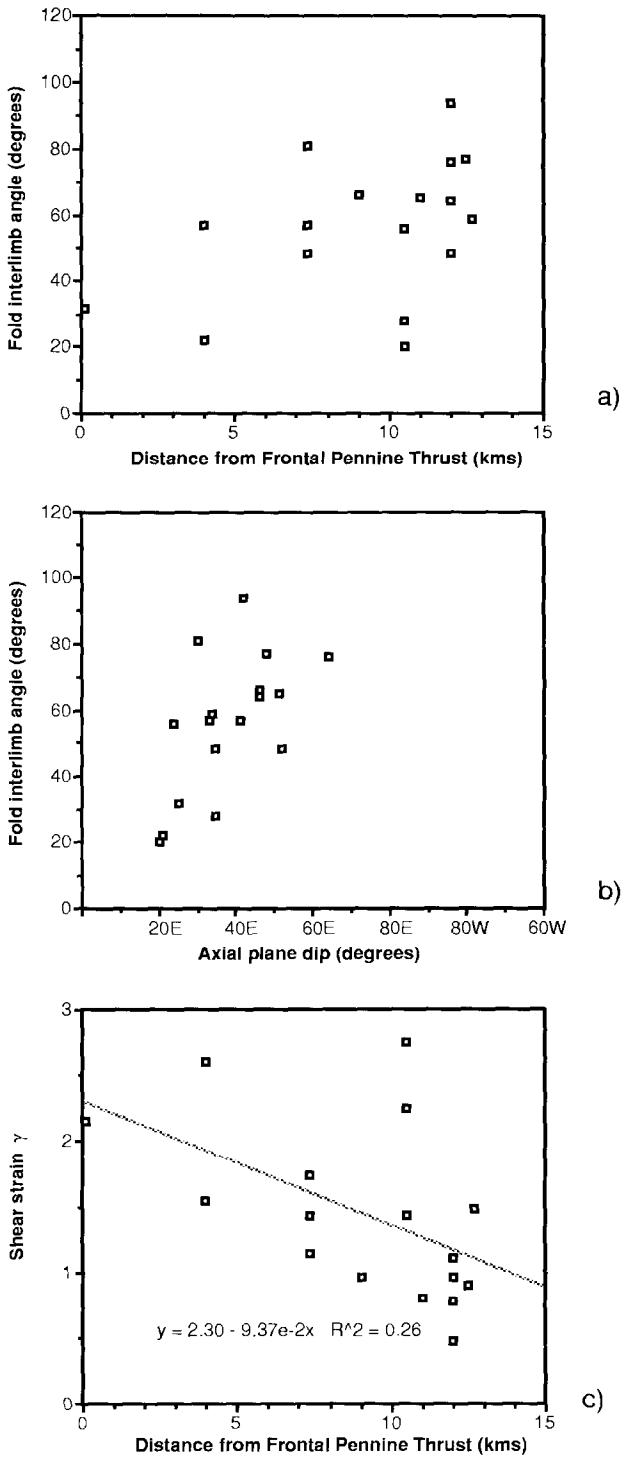

Fig. 9. (a)–(c) Plots of geometric parameters of the chevron folds in the southern domain. These data show the same relationships as in the Fournel profile (Fig. 7). (a) Fold interlimb angle vs distance from a fixed point on the Frontal Pennine Thrust. The values gradually decrease towards the Frontal Pennine Thrust. (b) Fold interlimb angle vs axial surface dip of the same folds. (c) Shear strain ($\gamma = \tan(90 - \alpha)$) vs distance from a fixed point on the Frontal Pennine Thrust.

the Pelvoux massif (Fig. 2) by Bravard (1982) who proposes that these are in stratigraphic position.

East of Orcières, large-scale folding ends in a regional open anticline (Orcières Anticline) which drops the top of the turbidite sequence ~1 km down to the west (Fig. 8a). We propose that this large NW–SE-trending anticline is related to a blind basement thrust (Orcières Thrust) which carries the hanging wall ~1 km towards the southwest. Further southwest, only rare minor (< 10 m) SW-vergent folds occur within the Tertiary sequence. This change in deformational style may be related to a change in the substrate. West of Orcières the Tertiary sequence is underlain by a thick sequence of Mesozoic rocks, especially the Middle to Upper Jurassic shales (Terres Noires), whereas east of Orcières the substrate is crystalline basement with local thin Triassic cover (Fig. 2). We speculate therefore that the blind Orcières Thrust is located on a paleo-normal fault (Fig. 8a).

Fault kinematic data from the Schistes à Blocs at Orcières (Fig. 8b) give SW-directed shortening within the Schistes à Blocs (Fig. 8c) and the Orcières Anticline and the Champsaur Thrust cut and involve the lower parts of the Embrunais–Ubaye nappes ('Schistes à Blocs' and Autapie nappe) (Figs 3 & 8; Kerckhove *et al.*, 1978). This implies that these lower units were emplaced over the Prapic fold zone during ongoing SW-directed deformation.

THE BASAL SHEAR ZONE: PROGRESSIVE SHEARING OF THE NUMMULITIC LIMESTONE AND GLOBIGERINA MARLS

Between the Grès du Champsaur and the crystalline basement lies a 5–60 m thick basal Tertiary sequence comprising local pockets of basal conglomerate, the Nummulitic Limestone and the Globigerina Marl. In general the basal conglomerates remain undeformed. The gradation between the two upper formations produces a smooth upward decrease in mechanical strength. The basal shear zone overprints this mechanical stratigraphy and can be divided into lower (Nummulitic Limestone), intermediate (transitional marly limestones) and upper (marls) levels with an upward increasing strain gradient. The basal Tertiary stratigraphy (and therefore the basal shear zone) is thicker (up to ~60 m) in the central domain (Fournel) than in the southern domain (22 m; Dormillouse). It also thins dramatically to the north of Fournel to less than 5 m in places. Structural data and characteristic synthetic profiles through the basal shear zone are shown on Fig. 10 (see also Plotto, 1977; Tricart, 1980). Small-scale structures in the basal shear zone record a history of progressive shear with a vertically increasing strain gradient. In order to describe this progressive deformation we have distinguished four generations of structures, numbered from B1 to B4. This numbering system is only applicable within the basal shear zone.

The main foliation (B1)

The main foliation (S_{B1}) is subparallel to bedding and carries a well developed stretching lineation. It is

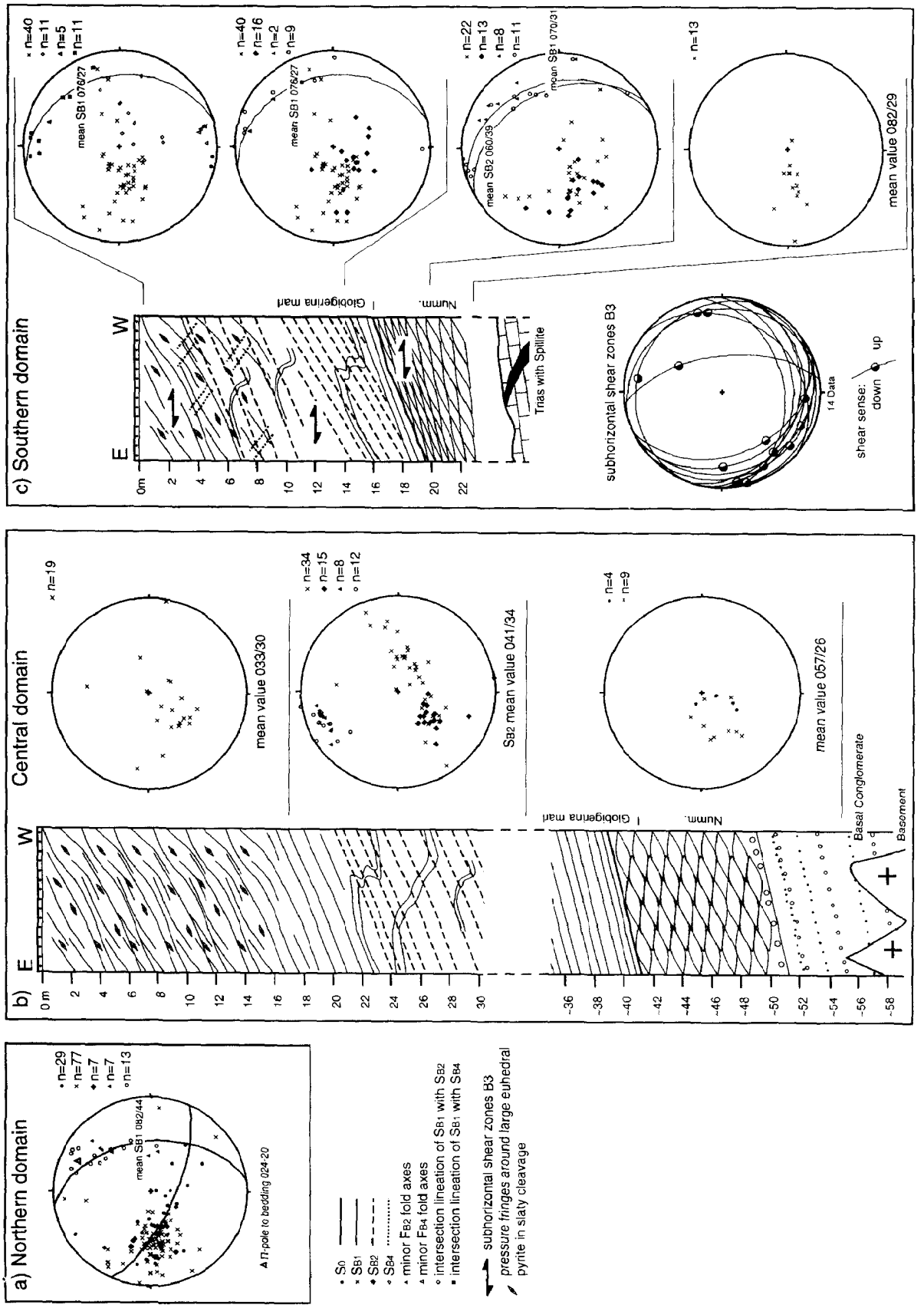

Fig. 10. B1–B4 structures in the basal shear zone across (a) the northern domain, (b) the central domain, and (c) the southern domain. The data include equal area lower hemisphere stereoplots and schematic vertical profiles across the basal formations in the central domain, and southern domain, showing the various fabrics and minor structures that develop in the shear zones and recording an upward increase in shear strain. Plot of B3 shear zones in (c). For further explanation see text.

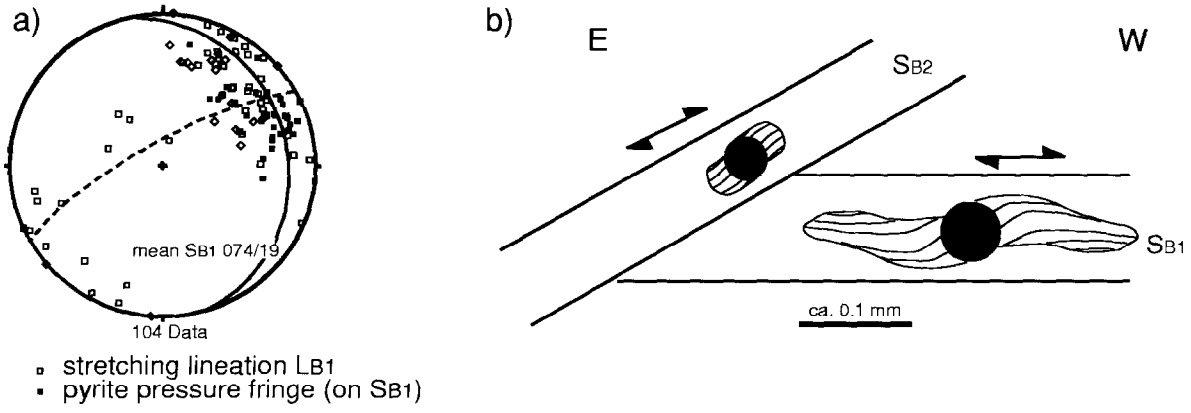

Fig. 11. Stretching lineations from the basal shear zone: (a) Equal area lower hemisphere projection plot of stretching lineation (L_{B1}) and pyrite pressure fringe data measured in the field on S_{B1} planes. Data from the whole area except the northernmost Chambran corner (see Fig. 15b). Most lineations and fringes lie on the mean S_{B1} great circle, some are folded by F_{B2} folds and fall on the dashed great circle. (b) Sketch showing the idealised shape and relationship to cleavage of pyrite pressure fringes observed in thin sections cut perpendicular to S_{B1} and parallel to the stretching lineation L_{B1}. Compare to Fig. 12(a).

not associated with any folding. Morphologically S_{B1} changes from a weak anastomosing cleavage in the lower level to a continuous cleavage in the intermediate, and slaty cleavage in the upper levels indicating a strong vertical deformational gradient (Fig. 10b & c). In areas of thinner basal Tertiary stratigraphy and thus higher shear strains, the spacing of S_{B1} decreases upwards within 5 m from ~6 cm to ~4 mm. In the central and southern domains S_{B1} dips around 30° towards the NE–ENE (Fig. 10b & c). In the northern domain, S_{B1} dips moderately east (Fig. 10a). In general the stretching lineation plunges northeast (Fig. 11a) with the exception of the northern domain where the stretching lineation changes to NW–SE- and N–S-trending (see below). In the lower levels the microlithons between the cleavage selvages are lozenge-shaped with the long axis subparallel to the stretching lineation on S_{B1}.

Euhedral pyrites in the upper level and small framboidal pyrites in the intermediate level often have antitaxial strain fringes. Most pressure fringes lie within S_{B1} but some short pressure fringes also occur within S_{B2} (see below) (Fig. 11b). Stretching lineation and quartz fibre orientations from larger pressure fringes (Figs 11a & 12a) clearly record a constant WSW–SW-directed stretching. The quartz fibres in the pressure fringes are slightly curved in the *XZ*-plane of finite strain recording a non-coaxial strain path (Figs 11b & 12a).

In thin section in the Globigerina Marl an original lamination has been accentuated by S_{B1} and consists now of ~1 mm thick fully recrystallized calcite-rich laminae (lozenge shaped grains ~30 μm long) separated by thinner pressure solution seams, variably enriched in phyllosilicates with a high degree of preferred orientation (< 0.2 mm wide) (Fig. 12b). Asymmetric tails around detrital grains (quartz, white mica, fossils) indicate top to west shearing and stretching within S_{B1} (Fig. 12c). In some places asymmetrical boudinage of phyllite rich pressure solution seams records ongoing stretching sub-parallel to the principal cleavage (Fig. 12d). S_{B1} slaty cleavage in the upper level of the basal shear zone is defined by the preferred orientation of aligned phyllosilicate grains, elongate quartz grains showing undulose extinction and interstitial calcite grains. In less strained areas, around heterogeneities, the slaty cleavage becomes anastomosing and domainal. Here the microlithon domains show some vestige of bedding (Fig. 12e).

Folding of the main foliation (B2)

In the intermediate level the bedding and S_{B1} cleavage are locally folded in asymmetrical WSW-vergent, mesoscale, gentle to open folds (F_{B2}; Fig. 13), causing the girdle distributions on pole plots of S_{B1} (Fig. 10). Amplitudes range from centimetres to decametres and wavelengths range from centimetres to few metres. In the central domain where strain is lowest, all F_{B2} fold axes plunge shallowly towards the NNW, perpendicular to the shear direction (Fig. 10b). In the northern domain and especially in the southern domain measured fold axes and intersection lineations (Fig. 10a & c) show a wide distribution of orientations which all fall on the great circle of the mean S_{B1} cleavage. In the field these F_{B2} fold axes are clearly curvilinear (Fig. 13e). The F_{B2} folds are associated with an axial planar cleavage (S_{B2}), expressed as cm-spaced, pressure solution seams. S_{B2} dips in the same direction as the mean S_{B1} (E–NE) but tends to be slightly steeper (Fig. 10). S_{B2} is best developed in the short limbs and hinge areas of F_{B2} folds, where the compositional layering $S_{0\text{-}B1}$ is thicker than in the surrounding rock mass (Fig. 13). Large amounts of material have been removed by pressure solution on S_{B2}, making compositional layering highly discontinuous (Fig. 13b). Slight buckling in the short limb of some F_{B2} folds results in second order forelimb-folds (Ray, 1991). The limbs of these second order folds are thinned (Fig. 13c). Some

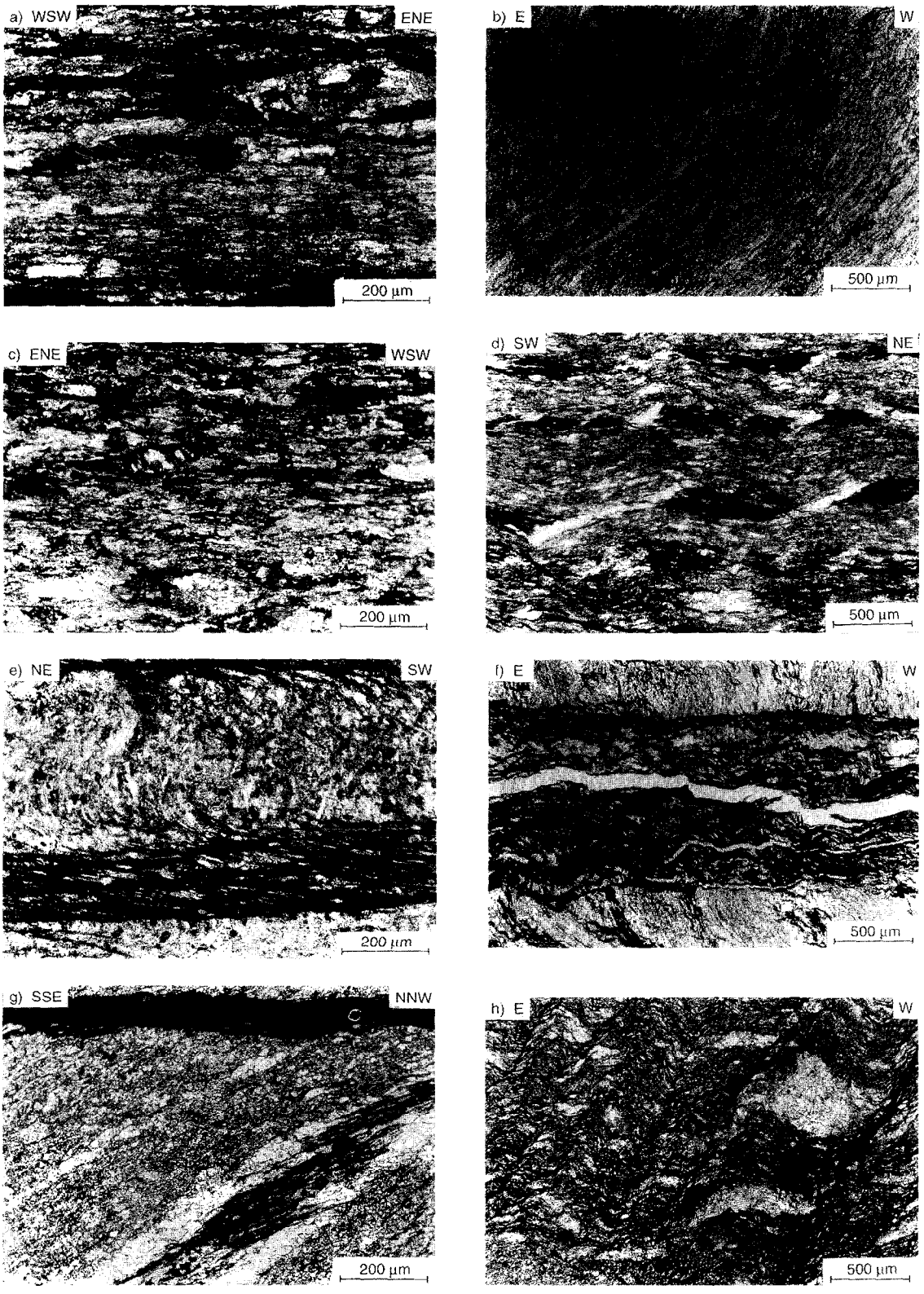

Fig. 12. Photomicrographs of thin sections cut perpendicular to S_{B1} and, unless stated otherwise, parallel to the stretching lineation L_{B1}. (a) Southern domain: spherical framboidal pyrite with quartz pressure fringe to the left and calcite fringe to the right in finer grained calcite matrix. S_{B1} (horizontal on this photograph) is marked by phyllosilicate seams. The quartz fibres in the pressure fringes rotated anticlockwise in sinistral non-coaxial flow while being pulled away from the pyrite. Calcite pressure fringes are also seen around fossil debris (in the lower left corner). Crossed polars (b) Southern domain: hinge area of an F_{B2} fold (cut perpendicular to fold axis); $S_{0\text{-}B1}$ lamination is defined by calcite separated by accumulations of phyllosilicates and insoluble residues. Elongate large calcite grains and pyrite pressure fringes lie subparallel to S_{B1}. The phyllosilicate rich seams are crenulated by S_{B2} (subhorizontal in this view). (c) Central domain: asymmetric tails around a quartz grain within a highly sheared S_{B1} fabric (give top to the west sense of shear). Crossed polars (d) Central domain: asymmetric boudinage of S_{B1} phyllosilicate seams (black) with interstitial growth of

F_{B2} mesofolds are localised on heterogeneities such as quartz–calcite veins (Fig. 13d). In these cases the fold amplitude dies out rapidly along the axial plane. The axial planar S_{B2} cleavage curves into sub-parallelism with the S_{B1} planes and spacing between seams decreases, until they are indistinguishable. At higher shear strains (i.e. in the southern domain), S_{B2} is omnipresent in the intermediate and upper levels and cleavage domains strongly dismember the F_{B2} folds (Fig. 13e). In the hinges of F_{B2} folds S_{B1} is well preserved in the microlithons and forelimb-folds are curvilinear. At Col de l'Aup Martin (Fig. 3), near the Selle-Fault, F_{B2} folds occur in a diminishing number indicating that the shear strain was lower.

In thin section S_{B2} generally forms dark throughgoing surfaces up to 2 mm wide, with aligned phyllosilicates and accumulations of insoluble residues (Fig. 12f). In some samples where S_{B2} is at a high angle to $S_{0\text{-}B1}$, small microfolds of S_{B1} are observed in the microlithons. In other cases S_{B2} develops as a crenulation cleavage associated with pressure solution (Fig. 12b). In the southern domain where S_{B2} is well developed, it can be observed in certain laminae that large calcite crystals (~0.1 mm long), aligned parallel to S_{B2}, grow over the S_{B1} pressure solution seams (Fig. 12g). Clear truncations at S_{B2} cleavage surfaces suggest that strong pressure solution took place along S_{B2}. Sigmoidally shaped $S_{0\text{-}B1}$ offsets at S_{B2} surfaces also indicate shearing on S_{B2} which may have caused the curvilinear shape of F_{B2} folds.

Sub-horizontal shear zones (B3)

In the northern and southern domains, higher shear strain leads to the development of discontinuous subhorizontal metre-scale shear zones in all levels (Fig. 10c). They cut through B1 and B2 structures (Fig. 13e). Slicken-fibre lineations on these shear surfaces and the curvature of older foliations indicate a top to the WSW-sense of shear (Fig. 10c). They are interpreted as shear bands (White *et al.*, 1980) which develop only in higher strain zones probably late in shear zone activity.

West-dipping cleavage (B4)

In the southern domain the principal foliation S_{B1} is locally cut by a west-dipping crenulation cleavage S_{B4} (Figs 10c & 14). Discontinuous bedding indicates a large amount of pressure solution. This cleavage is related to minor buckle folds with a thinned western limb (Fig. 14). The thinned limb sometimes merges into a distinct cleavage surface. No cross-cutting relations to B2 and B3 structures was found. The geometry makes it difficult to relate this structure to shear zone development. It is a very local feature and may be related to differential movement in the basement. Tricart (1980) suggested that this cleavage relates to late Alpine backthrusting, however, the very local distribution is not compatible with a regional event.

Chambran: transition to WNW-directed deformation

In Chambran, the narrow northernmost part of the Champsaur fold zone, the orientation of the stretching lineation in the basal shear zone changes northwards within 2 km, from NE–SW to NW–SE (Fig. 3) with a small number of N–S lineations measured within the transition zone. To the north at Rocher de l'Yret (Fig. 3) a series of WNW-directed (290°) thrusts in the footwall of the FPT carry basement onto Mesozoic and Tertiary cover (Butler, 1992a). B1 and B2 structural elements (Figs 10a & 15a) persist northward to location Y (Fig. 3). The F_{B2} folds are highly curvilinear. Within the transition zone (starred localities Fig. 3) additional metre-scale NNE–SSW-trending open folds occur in the upper level of the basal shear zone. They fold the $S_{0\text{-}B1}$ layering and are associated with an east dipping axial planar cleavage (Fig. 15a). Unfortunately no cross cutting relationship between the F_{B2} folds and these open folds could be observed but assuming that the F_{B2} structures are related to the WSW–SW-directed deformation we propose that the WNW-directed deformation was at least in part later because the open folds would have been obscured by the more intense B2 structures.

A model of progressive shear

The structures described (B1–B3) can be linked within a single progressive shear history. The principal S_{B1} cleavage and associated stretching lineation are the main fabrics produced within the shear zone. As shearing progressed, heterogeneities within the marls (such as veins) caused small asymmetrical folds to fold bedding, the principal cleavage and the stretching linea-

large calcite crystals (white). (e) Central domain: S_{B1} slaty cleavage (subhorizontal in photograph) with folded primary lamination preserved in a microlithon. (f) Southern domain: thick S_{B2} seam of phyllosilicates and insoluble residues crosscutting $S_{0\text{-}B1}$ (subvertical in photograph) in the hinge area of a F_{B2} fold. Differential crenulation cleavage dips steeply left (Selle-Fault cleavage) in the thick S_{B2} seam. Thin section cut perpendicular to the F_{B2} fold axis. (g) Southern domain: $S_{0\text{-}B1}$ fabric is oriented from top right to lower left corner. A thick S_{B2} seam is seen along the upper rim of the photograph. S_{B2} pressure solution cleavage is also intensely developed within the dark seam in the centre of the photograph (dipping left). Large rectangular calcite crystals are aligned subparallel to S_{B2} on either side of this seam. Thin section cut perpendicular to the F_{B2} fold axis. (h) Selle-Fault cleavage crenulating subhorizontal $S_{0\text{-}B1}$ fabric. Thin section cut perpendicular to the Selle-Fault folds.

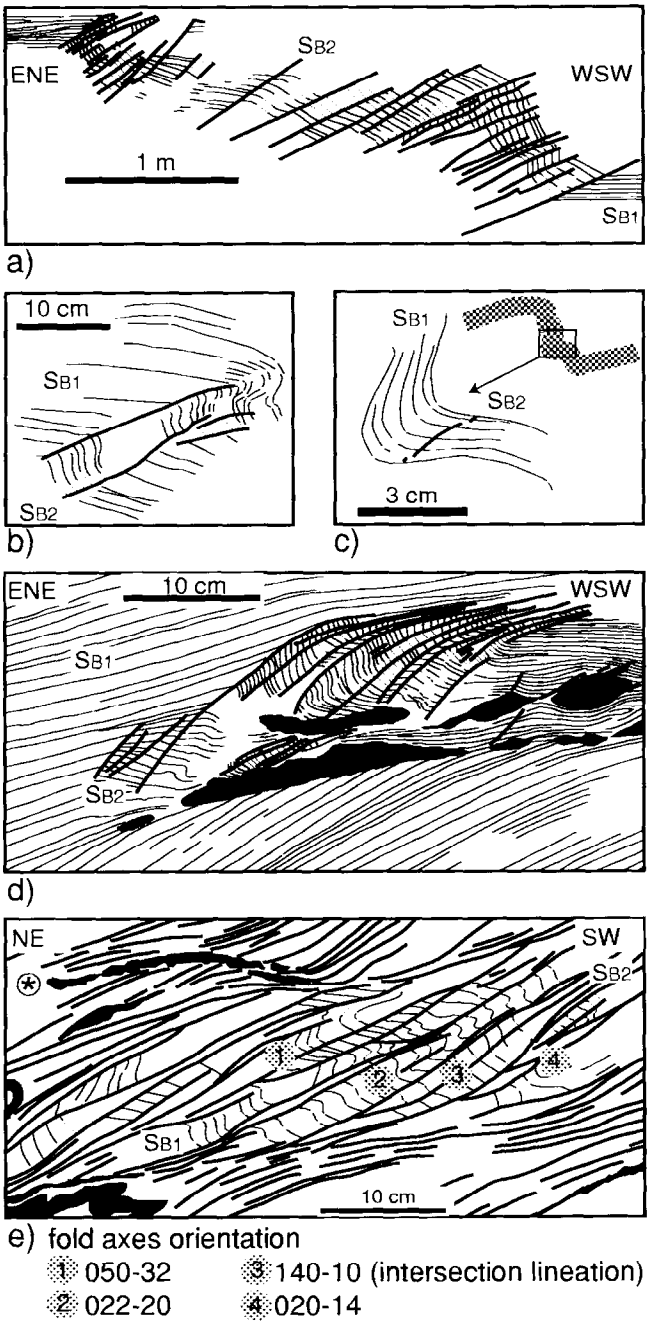

Fig. 13. Field sketches showing profile shapes of B2 folds in the basal shear zone. (a) (d) Examples from the central domain. (a) Large B2 folds with concentration of S_{B2} on the steep limbs. (b) Strong pressure solution on S_{B2} dissolves much of the fold hinge, which results in a highly discontinuous S_{B1}. (c) Detail from a second order forelimb fold showing thinning of the limbs. (d) B2 fold zone with strong S_{B2} localised on a quartz-calcite vein (black). Prior to F_{B2} the vein was boudinaged by the B1 deformation. The fold amplitude dies out rapidly along the axial plane until S_{B2} merges with S_{B1}. (e) B2 fold zone from the southern domain. S_{B2} dominates and strongly dismembers the fold hinge preserved in the microlithons. Minor fold hinges in such microlithons are highly curvilinear; see orientations of fold axes at localities 1–4. The orientation of fold axes varies from one microlithon to another. * Indicates a sub-horizontal B3 shear zone, marked by aligned quartz calcite veins (black).

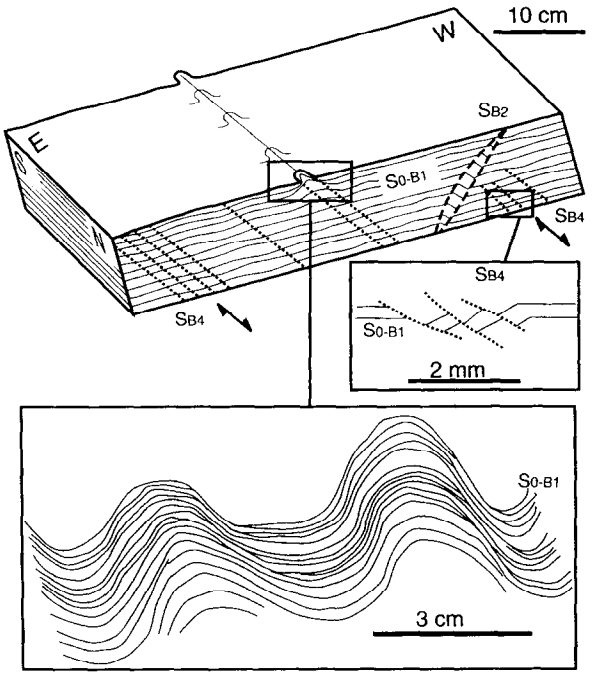

Fig. 14. Schematic block model showing the geometry and relationship of B4 structural elements to $S_{0\text{-}B1}$ and S_{B2}. Insets show thinning on F_{B4} limbs and apparent extensional geometries across some S_{B4}. For further explanation see text.

tion. Small flow perturbations were sufficient to rotate S_{B1} into the field of incremental shortening initiating S_{B2} and F_{B2} to accommodate the continuing shear strain (Gray, 1995). S_{B2}, a strong axial planar cleavage to these local (F_{B2}) folds merged with the continuously developing principal fabric $S_{0\text{-}B1}$ away from the folds. Where shearing became strong enough (e.g. in the northern and southern domains) the F_{B2} folds became curvilinear. F_{B2} folds, initially oriented almost perpendicular to the stretching direction, passively rotate towards the stretching direction (Donath and Parker, 1964). During later stage shear zone activity the large shear bands (B3) cut through B1 and B2 structures. They indicate a slightly east-dipping shear zone boundary subparallel to bedding. B1, B2 and B3 structures are thus genetically linked. Talbot (1964) and Laubach *et al.* (1989) report similar cleavage development in shear zones.

SELLE-FAULT

The NE–SW-trending Selle-Fault cuts mainly through basement and Mesozoic rocks and in a few places smaller satellite faults also affect Tertiary strata (Fig. 3). Slicken-fibres on brittle faults and shear zones, displaced veins, shear bands etc., all indicate oblique dextral shear which dropped the southern block down (Fig. 16a). Displacement on the Selle-Fault progressively increases towards the south from several tens of metres next to the FPT where the Selle-

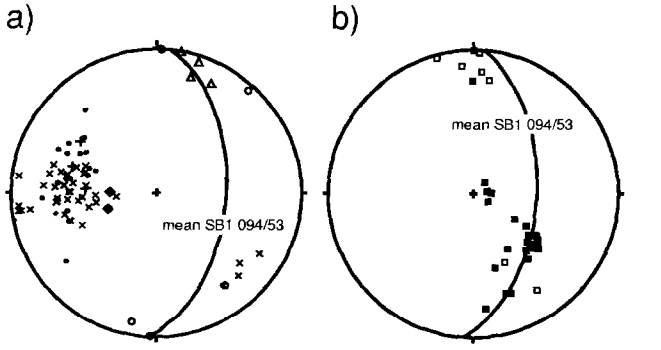

Fig. 15. Structural data from the basal shear zone at Chambran in the northern domain where the stretching lineation (L_{B1}) is N–S- to NW–SE-directed (Fig. 3): (a) Cleavage and bedding data. (b) Stretching lineation and pyrite pressure shadow data. Stretching directions which plunge north belong to the transition zone. Equal area lower hemisphere stereoplots.

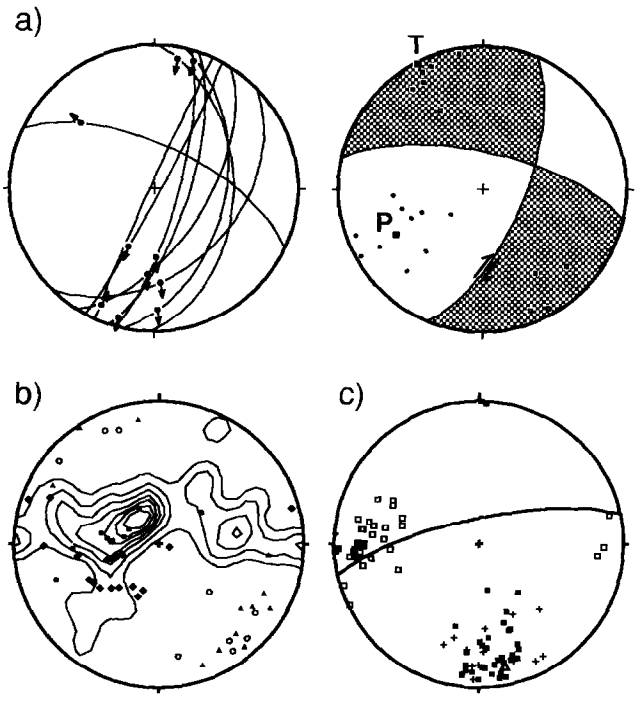

Fig. 16. Data from the basal shear zone at Col de l'Aup Martin (Fig. 3). Equal area lower hemisphere stereoplots. (a) Fault kinematic data from the Selle-Fault, raw data and fault plane solutions derived using the FaultKin programme of Allmendinger (1989–94). (b) B1 and B2 structural elements. (c) Orientation of Selle-Fault cleavage and Selle-Fault folds.

Fault bifurcates and individual branches die out (Fig. 3) (Barféty *et al.*, 1995) to ~0.9 km downthrow west of Orcières (Fig. 2) (Ford, 1996). This indicates that the Selle-Fault was of local significance during late Alpine deformation although it may have had an earlier history.

Observations from the basal shear zone at Col de l'Aup Martin (Fig. 3) show that near the Selle-Fault the F_{B2} folds (Fig. 16b) are overprinted by the Selle-Fault cleavage which is axial planar to metre-scale, upright, asymmetric, W-vergent folds with subhorizontal fold axes trending N–S (Figs 12h & 16c). These folds are clearly restricted to a narrow zone (< 1 km) close to the Selle-Fault though the Selle-Fault cleavage even occurs several km further east, as a very fine differentiated crenulation cleavage in thick pelitic seams (Fig. 12f). These structures are clearly related to a late dextral transtension on the Selle-Fault post-dating the basal shear zone.

INTERPRETATION AND DISCUSSION

Overthrust shear model

From the description above we can deduce that the deformation documented in the Fournel profile (Fig. 5) is due to one continuous deformation that was dominated by top to WSW overshear. A tectonic model for the Fournel profile must account for the geometrical information of large and small-scale structures. The main structural features which must be explained by any model are: (1) the progressive eastward change from large, open chevron folds with vertical axial planes to close, chevron-like folds with gently inclined axial planes (Fig. 5), (2) the positive correlation between interlimb angle and axial plane dip (Fig. 7b), (3) the concentration of folds in E-dipping zones which become shallower towards the east (Table 1), and (4) mesofolds and cleavage development in the basal shear zone. All these features reflect an increase in shear strain towards the hinterland (i.e. FPT) indicating that the shear strain was generated by emplacement of the overriding internal thrust sheets as previously suggested by Plotto (1977) and Tricart (1980).

This leads to an overthrust shear model (Fig. 17). The Champsaur fold zone offers a particularly well preserved record of overthrust shear deformation recording low shear strains ($\gamma \leq 3$; Fig. 7c) in a discrete zone sandwiched between rigid basement and the overthrusting mass. Along the Fournel profile the thickness of the Grès du Champsaur increases from ~700 m in the west near the Selle-Fault to ~1200 m approximately 8 km further east (Figs 5 & 8) giving the shear zone a wedge shaped profile. The development of folds in discrete zones whose dip decreases from vertical in the west to 20°E below the FPT (Table 1) requires further discussion. Restoration of folds across the Fournel profile causes the zone dips to increase but to preserve the same eastward decrease in

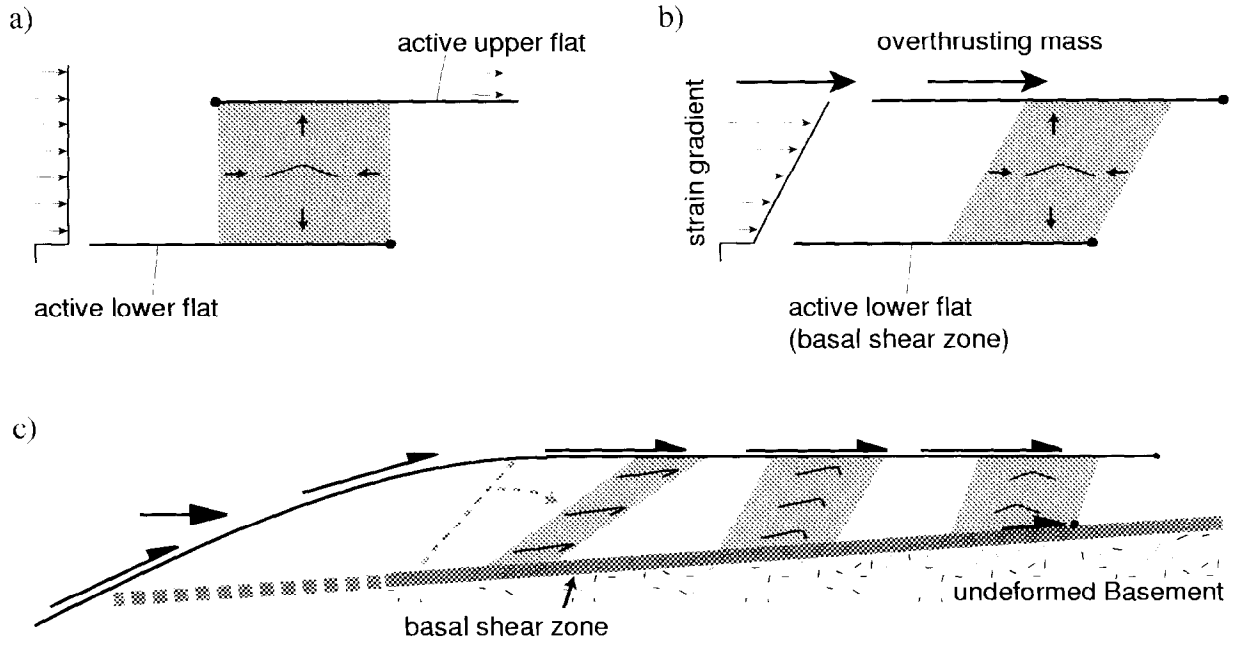

Fig. 17. Overthrust shear model. (a) Within a layered sequence deforming under pure shear a vertical diffuse ramp (shaded) develops by simultaneous movement on overlapping upper and lower flats. The diffuse ramp deforms in pure shear and leads to the initiation of buckle folds (modified after Casey and Dietrich, 1997). (b) Modification of (a). An increasing vertical strain gradient links the active lower flat (i.e. the basal shear zone) with the overthrusting mass. The lower flat lags behind the overthrusting mass. If the lower flat gets stuck, a diffuse ramp propagates upward through the layered sequence in which upright buckle folds initiate. The vertical strain gradient controls the dip of the diffuse ramps so that the higher the strain gradient between the floor and roof shear zones, the shallower the dip of a ramp that connects them. (c) Overthrust shear model for the Fournel profile depicted on Fig. 5. Wedge shaped turbidite sequence overlies the basal shear zone. The first diffuse ramp formed next to the overthrusting mass and sequentially newer ramps developed toward the foreland with progressively steeper dips. The initiated symmetric buckle folds rapidly amplified asymmetrically (Casey and Huggenberger, 1985). Continued shear further tightened and rotated the chevron folds and fold zones.

value, for example, the dip of zone E increases from 28° to 45° after restoration. This implies that the eastward decrease in zone-dip is an original feature. Casey and Dietrich (1997) propose that vertical zones of pure shear (diffuse ramps) can develop between overlapping upper and lower flats within a layered sequence deforming under pure shear (Fig. 17a). We propose an adaptation of this model in which: (1) the basal shear zone (below the Tertiary foreland succession) propagates forward in a position below and behind the overthrusting mass of internal nappes (Fig. 17b); (2) there is a decreasing vertical strain gradient downward between the FPT and the basal shear zone; (3) the basal shear zone from time to time sticks and a diffuse ramp propagates upward through the Tertiary sequence in which upright buckle folds initiate; (4) the vertical strain gradient controls the dip of the diffuse ramps so that the higher the strain gradient between the two sub-horizontal shear zones, the shallower the dip of a ramp that connects them (Fig. 17b); (5) once a diffuse ramp is initiated (at whatever angle) folding within it proceeds following the classic overthrust shear model (Fig. 1) and the zone itself is rotated to a shallower dip. This model implies that the vertical strain gradient diminishes westward until the most westerly diffuse ramp on the Fournel profile is vertical (Fig. 17c). Thus not only fold geometries but also the dip of the fold zones themselves record a decrease in overthrust shear deformation toward the west. Thus the strain gradient (from zone A to zone F; Fig. 5) represents the progressive development of structures through time and space (Fig. 17c). Similar observations of fold behaviour in the southern domain (Figs 8 & 9) allow us to propose that this model applies for the whole Champsaur–Prapic fold zone.

Previously documented overthrust shear examples may show zonal shear strain gradients similar to the Fournel profile (Bosworth and Vollmer, 1981; Rattey and Sanderson, 1982) or a vertical strain gradient within a nappe or thrust sheet (Fig. 1b) (Sanderson, 1979; Ramsay *et al.*, 1983; Gibson and Gray, 1985; Dietrich and Casey, 1989; Rowan and Kligfield, 1992; Casey and Dietrich, 1997).

In the first group of examples deformation in the footwall of an overthrusting mass is accommodated in listric zones of high shear strain shallowing downward (Rattey and Sanderson, 1982). Shear strain decreases forward and downward. Detailed structural observations are complicated by high shear strains and overprinting deformation phases. However, unlike in the Fournel profile the high strain zones do not ramp from a distinct floor shear zone but are unconstrained scattered shear zones which probably follow less competent rock assemblages. They are not controlled by a

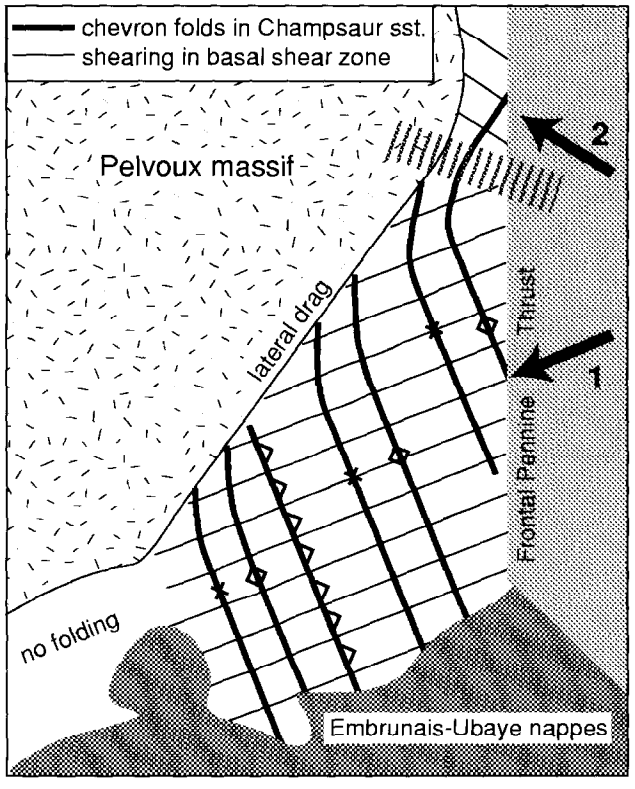

Fig. 18. Schematic map showing the large-scale relationship of structural elements at the southeast corner of the Pelvoux massif. Overthrust shear causes folding in the turbidite sequence and reorientation of fold axes by lateral drag against the proto-Pelvoux massif. Below the basal shear zone shows constant shearing towards the WSW–SW. To the north this shear direction changes to the northwest which is sub-perpendicular to the reoriented chevron folds. The northwest tectonic transport is partially later than the southwest transport. For further explanation see text.

restricted shear zone thickness. Therefore the boundary constraints and the distribution of easy glide horizons critically influence the shear strain distribution. In the second case, overthrust shear causes rapidly increasing strains towards the base of a thrust sheet. The shear strain concentration at the base can be so high that a nappe structure with an overturned lower limb forms (Fig. 1b). In the Fournel profile shear strains are too low and the stratigraphic pile was probably too thin to form a nappe.

Late Alpine transport directions and curvature of axial trends

In the external Alps the magnitude of late Alpine NW-directed shortening in the Northern Subalpine chains (>100 km) (Butler, 1992b and references therein) is far greater than the SW-directed shortening (~21.5 km) of the Southern Subalpine chains (Fry, 1989; Lickorish and Ford, 1998) (Fig. 2). The relationship between the NW- and SW-directed sectors around the external Alpine arc is controversial, for example, Platt *et al.* (1989) and Vialon *et al.* (1989) interpret the kinematic data as representing a continuous radial thrusting whereas Ricou and Siddans (1986) and Butler *et al.* (1986) distinguish the two transport directions. Ambiguous ages of kinematic data compound the problem. Therefore only structures involving Tertiary stratigraphy can give unambiguous late Alpine transport directions.

The Pelvoux massif lies in the core of the external arc (Ford *et al.*, 1995). To the north, late alpine transport directions are toward the WNW–NW (e.g. Serre *et al.*, 1985). To the south, in the present study area, transport directions are toward the WSW. As the most northerly sector of the WSW–SW-directed Southern Subalpine chains, the Champsaur–Prapic fold zone and the Dévoluy area to the west (Fig. 2; Meckel *et al.*, 1996) record relatively minor amounts of shortening (5 km and 3 km, respectively). Shortening increases southward toward Digne to ~21.5 km (Lickorish and Ford, 1998). Within the Champsaur area any northward change in tectonic transport direction may be of significance for arc dynamics.

The northward clockwise curve in map view by ~40° of fold axial trends in the Grès du Champsaur (Fig. 3) suggests variable transport directions which could be related to a regional radial transition of the thrusting direction. But in the basal shear zone the stretching lineation remains WSW-directed (except for the Chambran area) (Fig. 18). This suggests that the chevron folding of the Grès du Champsaur is affected by local perturbations whereas the basal shear zone structures document the regional undisturbed transport direction. The curvature of fold axial trends in the Grès du Champsaur may have been caused by lateral drag against the proto-Pelvoux massif (Tricart, 1980, 1981) and thus is unrelated to the Western Alpine arc. Similar processes may also be responsible for cleavage transection. We have argued above, that the Selle-Fault fabrics post-date all other structures in the basal shear zone and therefore could not cause bending of fold axes as suggested by Plotto (1977). Additionally the displacement on the Selle-Fault dies out towards the northeast where the curvature of axial trends becomes most marked.

In the northern domain around Chambran stretching lineations in the basal shear zone record the change from the NW-directed sector to the SW-directed sector of the external Alps in the immediate footwall of the FPT. We have argued that the WNW-directed deformation in part post-dates the WSW–SW-directed deformation at Chambran (Fig. 18). The change in orientation of the stretching lineation in the basal shear zone is not abrupt and is not segmented with any significant fault zone (Fig. 3). The northern termination of the Selle fault, which accommodates in total ~600 m of dextral displacement, lies to the north of the transition zone and cannot be used to partition the two transport directions. These two transport directions record the emplacement of the internal units onto the alpine foreland. As presented above, WNW–NW-directed shortening in the foreland is at least five

times greater than SW–WSW-directed shortening, implying that within the hanging wall of the FPT NW–WNW-directed deformation must be partitioned by strike-slip systems from the lesser WSW–SW-directed shortening. Models of this type have previously been proposed by Ricou and Siddans (1986) and Butler *et al.* (1986). The data presented in this paper do not support the model of radial thrusting (e.g. Platt *et al.*, 1989; Vialon *et al.*, 1989).

The problem of the hanging wall

Using the present Bureau de Recherche Géologiques et Minières (BRGM) geological maps, it is difficult to define which overthrusting nappe stack caused the WSW–SW-migrating overthrust shear recorded in the Champsaur–Prapic fold zone. Along the southern margin of the study area the fold zone is overlain by the Embrunais–Ubaye nappes emplaced along the FPT. The lower units of this nappe stack are involved in WSW-directed folding with the underlying foreland (Fig. 8). Further north, the FPT emplaces attenuated Sub-briançonnais units onto the foreland (Figs 2 & 3). Recent evidence (Tricart *et al.*, 1996) suggests that the FPT may have acted as a major detachment for late (Plio-Quaternary) extension within the internal zones, thus distorting its original thrust-relationship to the foreland. The tectonic relationship between the Embrunais–Ubaye nappes and the more internal units is unclear leading to several contradictory models for their emplacement onto the foreland (Kerckhove, 1969; Kerckhove *et al.*, 1978; Tricart, 1980, 1986; Merle and Brun, 1984; Fry, 1989). From our work we can say that the foreland records the progressive emplacement of a nappe stack toward the WSW. New data are awaited from the internal zones to clarify the identity of this overthrusting mass.

Acknowledgements—We thank Jean-Pierre Burg, Martin Casey and Joelle Lazarre for discussion. This study was supported by an ETH-project and by the Swiss National Science Foundation (Project No: 20-49534.96). We thank the office of the 'Pare National des Ecrins' for authorisation to work in the national park. Constructive reviews by Norman Fry and Pierre Tricart are acknowledged.

REFERENCES

Allmendinger, E. W., Marret, R. A. and Cladouhos, T. (1989–94) *FaultKin*, version 3.8a.

Aprahamian, J. (1974) La cristallinité de l'illite et les minéraux argileux en bordure des massifs cristallins externes de Belledonne et du Pelvoux (variations et relations possibles avec des événements tectoniques et métamorphiques alpins). *Géologie Alpine* **50**, 5–15.

Arnaud, H., Gidon, M. and Pairis, J.-L. (1977) Précisions sur la structure des chaînes subalpines méridionales dans la région de Faucon–Turriers–Clamensane (Alpes-de-Haute-Provence). *Géologie Alpine* **53**, 5–34.

Barféty, J.-C., Lemoine, M., Mercier, D., Polino, R., Nievergelt, P., Bertrand, J., Dumont, T., Amaudric du Chaffaut, S., Pêcher, A. and Monjuvent, G. (1995) *Carte géologique de la France (1/50,000), Feuille Briançon (823)*. BRGM, Orléans.

Barféty, J.-C., Pécher, A., Debelmas, J., Gidon, M., Mouterde, R., Vernet, J., Le Fort, P., Barbieri, A., Biju-Duval, J., Gillot-Barbieri, C., Bartoli, F. and Ozocak, R. (1984) *Carte géologique de la France (1/50,000). Feuille St.-Christophe-en-Oisans (822)*. BRGM, Orléans.

Beach, A. (1980) Some observations on the development of thrust faults in the Ultradauphinois Zone, French Alps. In *Thrust and nappe tectonics*, eds K. R. McClay and N. J. Price, pp. 335–352. Geological Society Special Publication **9**.

Bocquet, J. (1974) Colloque des 19–20 novembre 1973. Séance spécialisée de la Société Géologique de France: Le métamorphisme alpin dans les Alpes occidentales. *Géologie Alpine* **50**, 27–37.

Borradaile, G. J. (1978) Transected folds: a study illustrated with examples from Canada and Scotland. *Geological Society of America Bulletin* **89**, 481–493.

Bosworth, W. and Vollmer, F. W. (1981) Structures of the medial Ordovician flysch of eastern New York: deformation of synorogenic deposits in an overthrust environment. *Journal of Geology* **89**, 551–568.

Bravard, C. (1982) Données nouvelles sur la stratigraphie et la tectonique de la zone des Aiguilles d'Arves au Nord du Lautaret. *Géologie Alpine* **58**, 5–13.

Bruhn, R. L. (1979) Rock structures formed during back-arc basin deformation in the Andes of Tierra del Fuego. *Geological Society of America Bulletin* **90**, 998–1012.

Bürgisser, J. and Ford, M. (1997) Late stage geodynamics of an arcuate orogen as recorded by foreland basin deposits in the core of the external Alpine arc. *Terra Nova, abstract supplement* **9**, 320.

Butler, R. W. H. (1992a) Thrust zone kinematics in a basement-cover imbricate stack: Eastern Pelvoux massif, French Alps. *Journal of Structural Geology* **14**, 29–40.

Butler, R. W. H. (1992b) Thrusting patterns in the NW French subalpine chains. *Annales Tectonicae* **6**, 150–172.

Butler, R. W. H., Matthews, S. J. and Parish, M. (1986) The NW external Alpine Thrust Belt and its implications for the geometry of the Western Alpine Orogen. In *Collision Tectonics*, eds M. P. Coward and A. C. Ries, pp. 245–260. Geological Society Special Publication **19**.

Casey, M. and Dietrich, D. (1997) Overthrust shear in mountain building. In *Evolution of geological structures in micro- and macro-scales*, ed. S. Sengupta, pp. 119–142. Chapman & Hall, London.

Casey, M. and Huggenberger, P. (1985) Numerical modelling of finite-amplitude similar folds developing under general deformation histories. *Journal of Structural Geology* **7**, 103–114.

Coward, M. P., Gillcrist, R. and Trudgill, B. (1991) Extensional structures and their tectonic inversion in the Western Alps. In *The geometry of normal faults*, eds A. M. Roberts, G. Yielding and B. Freeman, pp. 93–112. Geological Society Special Publication **56**.

Debelmas, J., Le Fort, P., Biju-Duval, J., Vernet, J., Monjuvent, G., Beuf, S., Kerckhove, C. and Pêcher, A. (1980) *Carte géologique de la France (1/50,000). Feuille Orcières (846)*. BRGM, Orléans.

Debelmas, J., Lemoine, M., Kerckhove, C., Fail, J.-P., Lavergne, M., Leduc, J., Legreneur, J., Ortolfan, J., Robert, J.-P., Porié, R. and Gidon, M. (1966) *Carte géologique de la France (1/50,000). Feuille Guillestre (847)*. Service de la Carte Géologique de la France, Paris.

Dietrich, D. and Casey, M. (1989) A new tectonic model for the Helvetic nappes. In *Alpine tectonics*, eds M. P. Coward, D. Dietrich and R. G. Park, pp. 47–63. Geological Society Special Publication **45**.

Donath, F. A. and Parker, R. B. (1964) Folds and folding. *Bulletin of the Geological Society of America* **75**, 45–62.

Ford, M. (1996) Kinematics and geometry of early Alpine, basement-involved folds, SW Pelvoux Massif, SE France. *Eclogae geologicae Helvetiae* **89**, 269–295.

Ford, M., Meckel, L. D. and Bürgisser, J. (1995) Late Alpine kinematics around the Pelvoux massif, SE France: implications for arc geodynamics. *Terra Nova, abstract supplement* **7**, 274.

Fry, N. (1989) Southwestward thrusting and tectonics of the western Alps. In *Alpine tectonics*, eds M. P. Coward, D. Dietrich and R. G. Park, pp. 83–109. Geological Society Special Publication **45**.

Ghosh, S. K. (1966) Experimental tests of buckling folds in relation to strain ellipsoid in simple shear deformations. *Tectonophysics* **3**, 169–185.

Gibson, R. G. and Gray, D. R. (1985) Ductile-to-brittle transition in shear during thrust sheet emplacement, Southern Appalachian thrust belt. *Journal of Structural Geology* **7**, 513–525.

Gidon, M. (1965) Sur l'interprétation des accidents de la bordure méridionale du massif du Pelvoux. *Travaux du Laboratoire de Géologie de la faculté des sciences de Grenoble* **41,** 177–185.

Gidon, M. and Pairis, J.-L. (1980) Nouvelles données sur la structure des écailles de Soleil Boeuf (bordure sud du massif du Pelvoux). *Bulletin du Bureau de Recherches Géologique et Minières: série 2, section I* 35–41.

Gourlay, P. (1986) La déformation du socle et des couvertures delphino-helvétiques dans la région du Mont-Blanc (alpes occidentales). *Bulletin de la Société Géologique de France* **2,** 159–169.

Gray, D. R. (1995) Thrust kinematics and transposition fabrics from a basal detachment zone, eastern Australia. *Journal of Structural Geology* **17,** 1637–1654.

Johnson, T. E. (1991) Nomenclature and geometric classification of cleavage-transected folds. *Journal of Structural Geology* **13,** 261–274.

Kerckhove, C. (1969) La 'zone du Flysch' dans les nappes de l'Embrunais–Ubaye (Alpes occidentales). *Géologie Alpine* **45,** 5–204.

Kerckhove, C., Debelmas, J. and Cochonat, P. (1978) Tectonique du soubassement parautochtone des nappes de l'Embrunais–Ubaye sur leur bordure occidentale, du Drac au Verdon. *Géologie Alpine* **54,** 67–82.

Laubach, S. E., Reynolds, S. E. and Spencer, J. E. (1989) Progressive deformation and superposed fabrics related to Cretaceous crustal underthrusting in western Arizona, U.S.A. *Journal of Structural Geology* **11,** 735–749.

Lawson, K. (1987) Thrust geometry and folding in the Alpine structural evolution of Haute Provençe. Ph.D. thesis, University of Wales, Swansea.

Lickorish, H. and Ford, M. (1998) Sequential restoration of the external alpine Digne thrust system, SE France, constrained by kinematic data and synorogenic sediments. In *Cenozoic foreland basins of Western Europe*, eds C. Puidefabrigas and A. Mascle, pp. 189–211. Geological Society Special Publication.

Lory, P. (1894) Observations sur la coexistence dans le Massif de Chaillol de dislocations appartenant à deux périodes distinctes. *Compte-Rendu des Séances de la Société Géologique de France* **22,** CLXII–CLXIV.

Malavieille, J., Lacassin, R. and Mattauer, M. (1984) Signification tectonique des linéations d'allongement dans les Alpes occidentales. *Bulletin de la Société Géologique de France* **26,** 895–906.

Meckel, L. D., Ford, M. and Bernoulli, D. (1996) Tectonic and sedimentary evolution of the Dévoluy Basin, a remnant of the Tertiary western Alpine foreland basin, SE France. *Géologie de la France* **2,** 3–26.

Merle, O. and Brun, J. P. (1984) The curved translation path of the Parpaillon Nappe (French Alps). *Journal of Structural Geology* **6,** 711–719.

Pijolat, B., Gay, M., Gratier, J.-P. and Vialon, P. (1981) Les variations des valeurs de la déformation dans un système de plis par cisaillement. *Revue de Géologie Dynamique et de Géograpie Physique* **23,** 195–201.

Platt, J. P., Behrmann, J. H., Cunningham, P. C., Dewey, J. F., Helmann, M., Parish, M., Shepley, M. G., Wallis, S. and Weston, P. J. (1989) Kinematics of the Alpine arc and the motion history of Adria. *Nature* **337,** 158–161.

Plotto, P. (1977) Structures et déformations des "grès" du Champsaur au SE du massif du Pelvoux. Thèse 3e cycle. Université de Grenoble, France.

Ramsay, J. G., Casey, M. and Kligfield, R. (1983) Role of shear in development of the Helvetic fold–thrust belt of Switzerland. *Geology* **11,** 439–442.

Rattey, P. R. and Sanderson, D. J. (1982) Patterns of folding within nappes and thrust sheets: examples from the Variscan of southwest England. *Tectonophysics* **88,** 247–267.

Ray, S. K. (1991) Significance of forelimb folds in the Shumar allochthon, Lesser Himalaya, eastern Bhutan. *Journal of Structural Geology* **13,** 411–418.

Ricou, L. E. and Siddans, A. W. B. (1986) Collision tectonics in the Western Alps. In *Collision Tectonics*, eds M. P. Coward and A. C. Ries, pp. 229–244. Geological Society Special Publication **19.**

Ridley, J. and Casey, M. (1989) Numerical modeling of folding in rotational strain histories: strain regimes expected in thrust belts and shear zones. *Geology* **17,** 875–878.

Rowan, M. G. and Kligfield, R. (1992) Kinematics of large-scale asymmetric buckle folds in overthrust shear: an example from the Helvetic nappes. In *Thrust tectonics*, ed. K. R. McClay, pp. 165–173. Chapman & Hall, London.

Sanderson, D. J. (1982) Models of strain variation in nappes and thrust sheets: a review. *Tectonophysics* **88,** 201–233.

Sanderson, D. J. (1979) The transition from upright to recumbent folding in the Variscan fold belt of southwest England: a model based on the kinematics of simple shear. *Journal of Structural Geology* **1,** 171–180.

Serre, A., Toury, A., Rampnoux, J.-P., Reyes-Martinez, J. and Tardy, M. (1985) Individualisation de deux unités à flysch nummulitique d'origines paléogéographiques différentes au sein de "l'Ecaille ultradauphinoise des Aiguilles d'Arves" (région de Saint-Jean-de-Maurienne, Savoie). *Comptes rendus de l'Académie des Sciences, Paris* **301,** 637–642.

Sinclair, H. D. (1997) Tectonostratigraphic model for underfilled peripheral foreland basins: an Alpine perspective. *Bulletin of the Geological Society of America* **109,** 324–346.

Spencer, S. (1992) A kinematic analysis incorporating incremental strain data for the Frontal Pennine Zones of the western French Alps. *Tectonophysics* **206,** 285–305.

Talbot, J. L. (1964) Crenulation cleavage in the Hunsrückschiefer of the middle Moselle region. *Geologische Rundschau* **54,** 1026–1043.

Tanner, P. W. G. and Macdonald, D. I. M. (1982) Models for the deposition and simple shear deformation of a turbidite sequence in the South Georgia portion of the southern Andes back-arc basin. *Journal of the Geological Society of London* **139,** 739–754.

Tricart, P. (1986) Le chevauchement de la zone briançonnaise au Sud-Est du Pelvoux: clé des rapports zone externe–zones internes dans les Alpes occidentales. *Bulletin de la Société Géologique de France* **2,** 233–244.

Tricart, P. (1984) From passive margin to continental collision: a tectonic scenario for the Western Alps. *American Journal of Science* **284,** 97–120.

Tricart, P. (1981) Les marqueurs des movements verticaux du socle aux abords du massif du Pelvoux (Alpes occidentales). *Revue de Géologie Dynamique et de Géograpie Physique* **23,** 289–300.

Tricart, P. (1980) Tectoniques superposées dans les Alpes occidentales au Sud du Pelvoux: évolution structurale d'une chaîne de collision. Ph.D. thesis, Université de Strasbourg, France.

Tricart, P., Bouillin, J. P., Dick, P., Moutier, L. and Xing, C. (1996) Le faisceau de failles de haute-Durance et le rejeu distensif du front briançonnais au SE du Pelvoux (Alpes occidentales). *Comptes rendus de l'Académie des Sciences, Paris* **323,** 251–257.

Vialon, P., Rochette, P. and Ménard, G. (1989) Indentation and rotation in the western Alpine arc. In *Alpine Tectonics*, eds M. P. Coward, D. Dietrich and R. R. G. Park, pp. 329–338. Geological Society Special Publication **45.**

Waibel, A. F. (1990) Sedimentology, petrographic variability, and very-low-grade metamorphism of the Champsaur sandstone (Paleogene, Hautes-Alpes, France). Evolution of volcaniclastic foreland turbidites in the external Western Alps. Ph.D. thesis, Université de Genève, Suisse.

White, S. H., Burrows, S. E., Carreras, J., Shaw, N. D. and Humphreys, F. J. (1980) On mylonites in ductile shear zones. *Journal of Structural Geology* **2,** 175–187.